NASA CR-54137

DEVELOPMENT OF A MINIATURE ELECTROSTATIC ACCELEROMETER (MESA) FOR LOW g APPLICATIONS

by

M.A.Meldrum, E.J.Harrison, and Z.Milburn

prepared for

NATIONAL AERONAUTICS AND SPACE ADMINISTRATION

CONTRACT NAS 3-4102

BELL AEROSYSTEMS COMPANY

DIVISION OF BELL AEROSPACE CORPORATION-A textron COMPANY

NOTICE

This report was prepared as an account of Government sponsored work. Neither the the United States, nor the National Aeronautics and Space Administration (NASA), nor any person acting on behalf of NASA:

A.) Makes any warranty or representation, expressed or implied, with respect to the accuracy, completeness, or usefulness of the information contained in this report, or that the use of any information, apparatus, method, or process disclosed in this report may not infringe privately owned rights; or

B.) Assumes any liabilities with respect to the use of, or for damages resulting from the use of any information, apparatus, method or process disclosed in this report.

As used above, "person acting on behalf of NASA" includes any employee or contractor of NASA, or employee of such contractor, to the extent that such employee or contractor of NASA, or employee of such contractor prepares, disseminates, or provides access to, any information pursuant to his employment or contract with NASA, or his employment with such contractor.

Requests for copies of this report should be referred to

National Aeronautics and Space Administration
Office of Scientific and Technical Information
Attention: AFSS-A
Washington, D.C. 20546

NASA CR-54137
BAC 60009-509

SUMMARY REPORT

DEVELOPMENT OF A MINIATURE ELECTROSTATIC ACCELEROMETER (MESA) FOR LOW g APPLICATIONS

by

M.A. Meldrum, E.J. Harrison, and Z. Milburn

prepared for

NATIONAL AERONAUTICS AND SPACE ADMINISTRATION

April 30, 1965

CONTRACT NAS 3-4102

Technical Management
NASA Lewis Research Center
Cleveland, Ohio
Spacecraft Technology Division
Bernard L. Sater

BELL AEROSYSTEMS COMPANY
P.O. Box 1
Buffalo 5, New York

DEVELOPMENT OF A MINIATURE ELECTROSTATIC ACCELEROMETER (MESA) FOR LOW g APPLICATIONS

by

M. A. Meldrum, E. J. Harrison, and Z. Milburn

ABSTRACT

A miniature, single-degree-of-freedom digital electrostatic accelerometer (MESA) has been developed for measurement of accelerations in the 10^{-3} to 10^{-12} g range. The design, fabrication, and qualification test results of the MESA are discussed in this Summary Report.

DEVELOPMENT OF A MINIATURE ELECTROSTATIC ACCELEROMETER (MESA) FOR LOW g APPLICATIONS

by

M. A. Meldrum, E. J. Harrison, and Z. Milburn

SUMMARY

Under the sponsorship of the NASA Lewis Research Center, Spacecraft Technology Division, a Miniature Electrostatic Accelerometer (MESA) has been developed by Bell Aerosystems Company Products and Instruments Group.

The program, initiated in August, 1963, had as its objective the development of a digital accelerometer capable of accurately measuring accelerations in the 10^{-3} to 10^{-6} g range. The accelerometer was required to withstand, without degradation in performance, high launch vibration and shock conditions of the Thor-Delta vehicle, and to operate reliably over long periods of time in an orbiting environment. To achieve those objectives, two miniaturized versions of the digital Electrostatic Accelerometer (ESA) developed under Air Force Contract AF33(616)-6637 were designed, fabricated, and tested.

Although the evaluation of accelerometer performance in the low g range is limited in part by the requirement that laboratory tests must be conducted in a 1 g environment, significant performance data was obtained. Test results showed:

(1) Long term scale factor variation of less than 3×10^{-7} g for 10^{-3} g input.

(2) Scale factor temperature coefficient of 7×10^{-7} g/°F for 10^{-3} g input.

(3) Long term null variations of less than $\pm 5 \times 10^{-7}$ g for 1g suspension.

(4) Null temperature coefficient of less than 3×10^{-6} g/g/° for 1 g suspension.

The MESA also demonstrated that it is capable of sustaining (without performance degradation) 40 g peak acceleration and 15 g shock.

This program has enabled the accurate measurement of very low accelerations to be made by an accelerometer also capable of withstanding a wide range of high g launch environments. It has also established that the variable range electrostatic suspension and digital constrainment concept is one which offers a practical solution to accurate low g measurements.

The major task remaining is the evaluation of the MESA performance characteristics in a low g (10^{-6} to 10^{-12} g) rather than 1 g test environment; this could be accomplished in an orbital experiment. A successful evaluation would enable the MESA to be used in an even greater variety of spacecraft guidance and control applications where accelerations of 10^{-6} to 10^{-12} g range are encountered. Typical of these applications are:

(1) Spacecraft gravity gradient attitude stabilization and control.

(2) Spacecraft orbital alignment and compassing.

(3) Measurement of orbital parameters such as eccentricity, true anomaly and semi-major axis.

(4) Spacecraft drag and thrust measurement for synchronous orbit station-keeping.

(5) Measurement of gravity of the earth, moon, and planets.

(6) Interplanetary trajectory velocity control.

CONTENTS

CONTENTS (CONT)

ILLUSTRATIONS

SECTION 1.0
INTRODUCTION

The requirement for an accelerometer capable of measuring accelerations in the 10^{-3} to 10^{-12} g range was recognized by Bell Aerosystems Company in 1959. Accelerometers of this type would find extensive use in orbital guidance and control of spacecraft where the accurate measurement of low g levels would be required. A conventional force balance accelerometer such as the Bell Model IIIB could not be used in this application because of limited null stability and repeatability. This limitation is due to the cross-coupling of the mechanical suspension forces into the instrument sensitive axis. The accelerometer mechanical suspension system must also be capable of withstanding the maximum cross-axis g under launch conditions (up to 100 g). However, in a low g environment, little suspension force is required. Since it is not possible to easily change the mechanical suspension force, a conventional instrument is limited to measurements in the 10^{-5} to 100 g range.

To overcome this problem, Bell Aerosystems undertook a program to develop an accelerometer whose acceleration sensing proof mass was suspended and constrained by electrostatic forces whose magnitude could be changed to meet the operating g environment by a simple change in suspension and constrainment voltage levels. Under the sponsorship of the Guidance Division, Air Force Avionics Laboratory, Research and Technology Division, Air Force Systems Command, Wright Patterson Air Force Base, Ohio, a development program was initiated in 1959 and completed in 1963 under contract AF33(616)-6637. The feasibility of the electrostatic accelerometer concept was demonstrated and four experimental models tested.

The ESA developed had the following characteristics:

(1) Single-degree-of-freedom.

(2) Acceleration sensing proof mass was suspended and constrained by electrostatic forces.

(3) Sensitive axis constrainment was achieved by pulse force rebalance techniques.

(4) Instrument g scaling was adjustable by simple change in signal level.

(5) Output was a digital pulse rate proportional to acceleration.

(6) Accelerometer was capable of withstanding high g loads without performance degradation.

Under sponsorship of the NASA Lewis Research Center, a program (details of which are presented in this report) was undertaken to develop two flight qualified miniature versions of the electrostatic accelerometer (MESA) for measurement of accelerations in the 10^{-4} to 10^{-6} g range. Significant improvements and refinements were made in both electronic and mechanical design. The accelerometer size was reduced by half without compromising performance. The electronics for the power supply, pickoff and pulse constrainment system, suspension system, and temperature controls were designed and fabricated as welded modules and tested. The MESA system was successfully tested under typical launch and simulated orbital environments.

The remaining sections in this report discuss the theoretical, experimental, and practical aspects of the MESA program. Conclusions and recommendations are given at the end of the report.

SECTION 2.0

TECHNICAL DESCRIPTION

The basic design philosophy of the MESA assumes a dynamic range of 10^{-6} (the ratio of minimum measurable input to maximum measurable input) as representative of the state-of-the-art. Today, the low g range requirement does not in itself require immediate advance in the state-of-the-art, provided the dynamic range remains the same. Therefore, an instrument with a range of, for example, 10^{-11} to 10^{-5} g is within the state-of-the-art.

The minimum measurable acceleration is the function of the coupling of the suspension system into the sensitive axis. To lower the minimum measurable acceleration, the suspension system must be weakened. This can be accomplished easily in an electrostatic suspension system by reducing the suspension voltage. The basic concept is to use an electrostatic system which will permit adjustment and calibration in the one g field of the earth and to switch the suspension voltage to a lower value for measuring in-space acceleration environments.

2.1 DESCRIPTION OF THE BASIC INSTRUMENT (Figures 1 and 2)

The proof mass is a hollow cylindrical float which has a flange around the center. The cylinder is supported by eight electrodes arranged to act against the inner surface of the float. Each electrode is in series with a tuning inductor which exerts a voltage across the electrode-float gap which is a function of the float position. The float position determines the capacity in a series tuned circuit and, therefore, the operating point on the series resonance characteristic curve. As a result of this situation, an attractive force develops between the float and electrode which increases as the float moves away from the electrode, causing the float to be suspended in all directions except along the cylindrical axis. The suspension system therefore centers the float under angular and translational accelerations. The suspension sweep oscillator and amplifiers provide automatic suspension of the float without voltage breakdown or arcing.

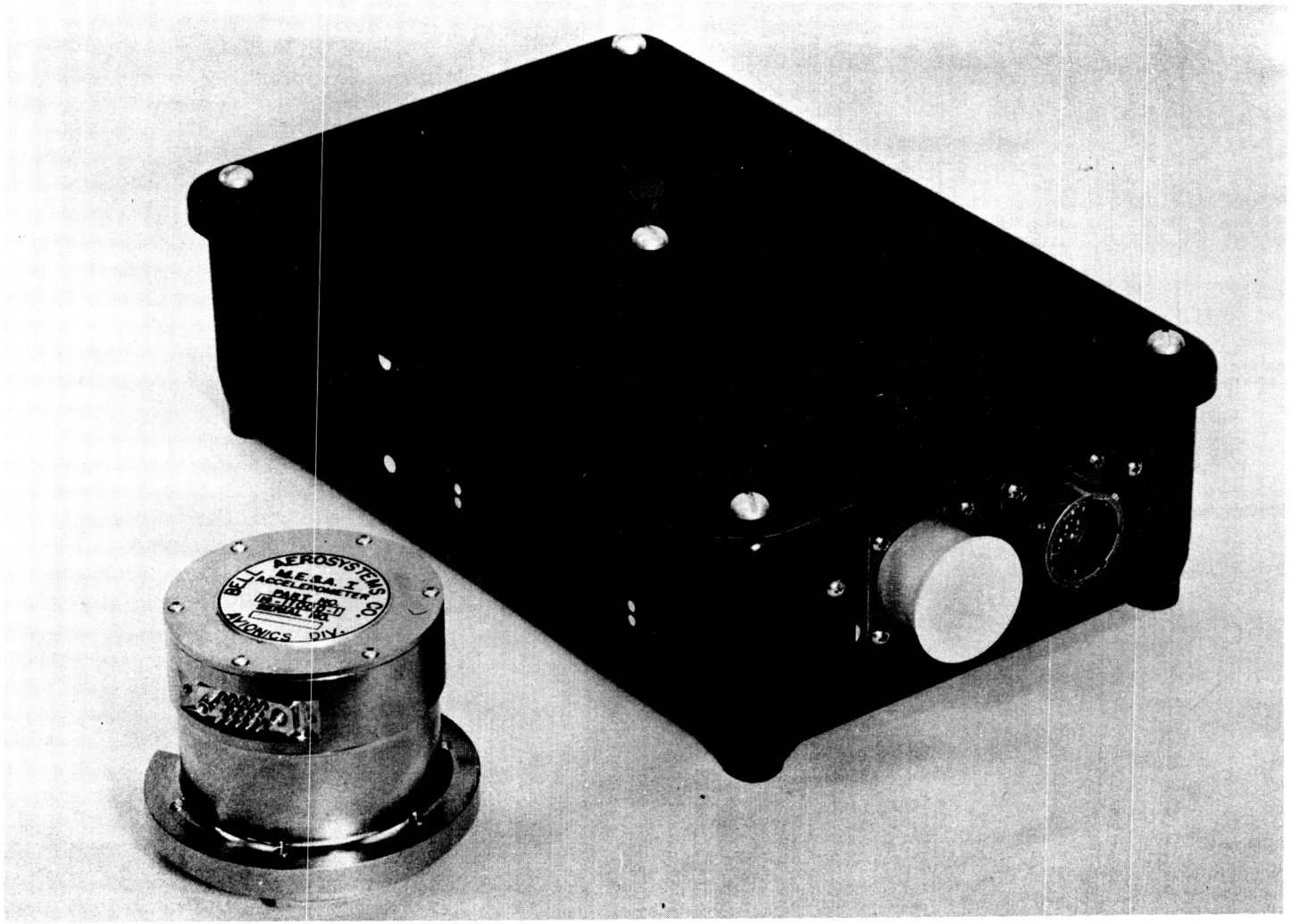

Figure 1. MESA IA System

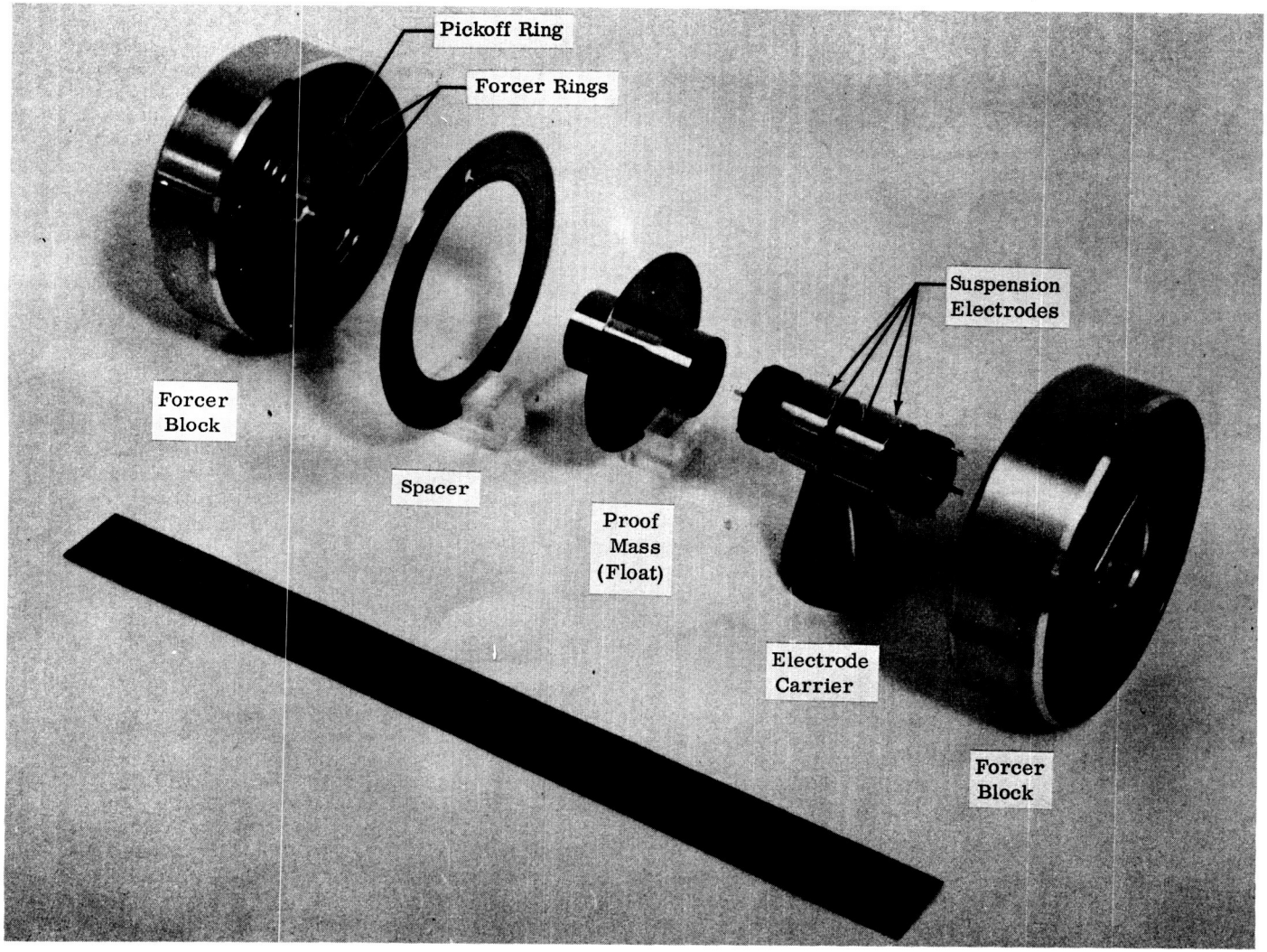

Figure 2. Primary Mechanical Elements

Detection of the float movement is accomplished by sensing the change in capacity between the pickoff ring concentric with the float flange. When used in a balanced capacitive bridge circuit excited by a carrier frequency, displacement of the float results in a signal output from the bridge. This output is amplified and phase sensitive demodulated to produce a d-c voltage whose polarity is a function of the direction of the float movement and whose amplitude is a measure of the relative displacement of the accelerometer null position. This voltage, when applied to the trigger circuit, results in the generation of d-c pulses which restrain the float. The d-c level at which pulsing starts is called the trigger level.

The forcing of the float along the sensitive (cylindrical) axis is accomplished by rings which form a capacity to the float flange. Voltage pulses are applied to these rings in a similar manner to force along the sensitive cylindrical axis. The pulses are generated by a pulse core which controls the amplitude and width of the pulse. This pulse generation technique is presently used on digital velocity meters for the Agena program and its accuracy and stability have been verified in many space flights. The system output information is a pulse rate proportional to acceleration.

2.2 THEORY OF OPERATION

2.2.1 Suspension System

The basic principle for suspending the accelerometer utilizes the force between the charges from the plates of the capacitor. The attractive force tends to move the plates toward each other. This electrostatic force is given by the equation

$$F = \frac{KV^2A\ (10^{-4})}{8\pi\ \delta^2 9} \quad \text{dynes} * \qquad (1)$$

where

K = Dielectric constant (assumed to be unity)

V is the voltage across the plate (volts)

A is the area of the plates (cm^2)

δ is the gap between the plates (cm)

*Edgcumbe, K., and Ockender, F.E.J., "Industrial Electrical Measuring Instruments," Sir Isaac Pitman and Sons Ltd., London, 1933, pg. 207.

If the equation is expanded, the force per unit area can be written

$$\frac{F}{A} = 4.42 \times 10^{-7} \left(\frac{V}{\delta}\right)^2 \frac{\text{dynes}}{\text{cm}^2} \tag{2}$$

With fixed voltages on the capacitor plates, the attractive force increases as δ decreases which is not the action needed for the suspension system. To overcome this effect, constrainment is effected using an a-c voltage applied to a resonant circuit consisting of an inductance in series with the capacitance. The voltage across the gap will vary as the gap changes, decreasing as the gap decreases if the operating frequency f is slightly above the resonant frequency f_o.

Consider the single-degree-of-freedom suspension system shown in Figure 3. The resonant frequency corresponds to the value for a centralized float. The following equations are derived.

The voltage across each gap can be shown to be

$$V_{c1}^2 \quad \frac{E^2 (1+u)^2}{\left[1 - (f/f_o)^2 + u\right]^2 + \left[\frac{f/f_o}{Q_o}\right]^2} \quad \text{volts}^2 \tag{3}$$

where

C_o = $\frac{KA}{\delta}$ centralized gap capacity (farads)

L = tuning inductance (henry)

f_o = $\frac{1}{2\pi\sqrt{LC_o}}$ resonant frequency

Q_o = $\frac{2\pi f_o L}{R} \cong 40$

R = series resistance (ohms)

E = suspension excitation (volts)

u = $\frac{x}{\delta}$ = normalized float displacement

V_{c1} = voltage across electrode 1

V_{c2} = voltage across electrode 2

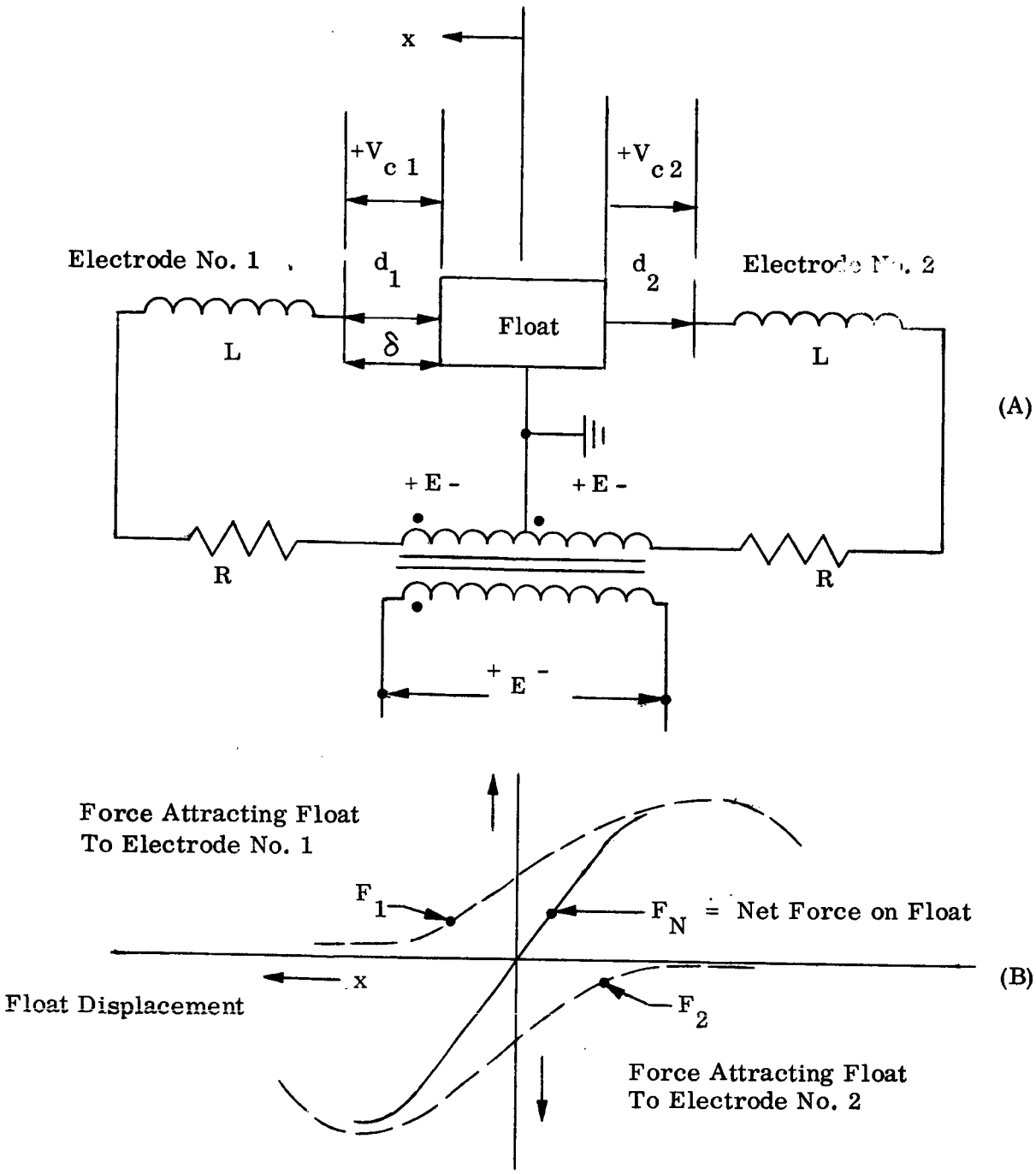

Figure 3. Single-Degree-of-Freedom Suspension System

$$V_{c2}^2 = \frac{E^2 (1-u)^2}{\left[1 - (f/f_o)^2 - u\right]^2 + \left[\frac{f/f_o}{Q_o}\right]^2} \text{ volts}^2 \quad (4)$$

This derivation is based on the float being at ground potential. The net force acting in a direction to restore the float to its equilibrium position is given by

$$F_N = K_f \left[\left(\frac{V_{c2}}{d_2}\right)^2 - \left(\frac{V_{c1}}{d_1}\right)^2\right] \text{ dynes} \quad (5)$$

where

$d_1 = \delta - x = \delta\ (1 - u)$ = gap between electrode 1 and float (cm)

$d_2 = \delta + x = \delta\ (1 + u)$ = gap between electrode 2 and float (cm)

Substituting (3) and (4) in (5)

$$F_N = \frac{K_f E^2}{\delta^2}\left[\frac{4\left(1 - (f/f_o)\right)^2}{\left[\left(1 - (f/f_o)^2 + u\right)^2 + \left(\frac{f/f_o}{Q_o}\right)^2\right]\left[\left(1 - (f/f_o)^2 - u\right)^2 + \left(\frac{f/f_o}{Q_o}\right)^2\right]}\right] \text{dynes} \quad (6)$$

If the operating frequency f is selected such that

$$f = f_o\ \left(1 + \frac{1}{2Q_o}\right) \quad (7)$$

Equation (6) reduces to

$$F_N = \frac{K_F E^2\ Q_o^3 u}{\delta^2 \left(1 + \frac{(Q_o u)}{4}\right)^4} = \frac{F_o Q_o^3 u}{1 + \frac{(Q_o u)}{4}^4} \text{ dynes} \quad (8)$$

2.2.2 Suspension of a Cylinder

A flanged cylindrical proof mass and an eight electrode suspension system has the following properties. The suspension forces are normal to the instrument sensitive axis. Restraint is provided against both translation and rotation in the two transverse axes. The eight electrode configuration makes use of a balanced

suspension excitation with adjacent electrodes exicted by equal voltages 180° out of phase. This latter characteristic assures that the float will be very near ground potential. Since all forces are normal to the surface of the cylinder wall, an equivalent force diagram may be drawn as shown in Figure 4.

Neglecting stray capacity and assuming equal suspension capability for each electrode, the resultant total force (see Figure 4) is

$$F_N = ma \text{ dynes} \tag{9}$$

where

F_N = electrode suspension force assumed to act at an angle 45° as shown

m = mass of float grams

a = acceleration applied to floats

From equation (8)

$$\frac{K_f E^2 Q_o{}^3 u}{\delta^2 \left[1 + \frac{(Q_o u)^4}{4}\right]} = \frac{ma}{2\sqrt{2}} \tag{10}$$

If $\frac{(Q_o u)^4}{4} << 1$ (required also for stability of suspension system)

$$u = \frac{ma\,\delta^2}{2\sqrt{2}\left[4.42 \times 10^{-7}\right] A Q_o{}^3 E^2} \tag{11}$$

For given values of m, δ, A, Q_o, the displacement of the float from its centralized positiom may be found for various values of E and a. Conversely, for a given u and a, the suspension excitation required may be found.

2.2.3 Sensitive Axis Restrainment

The basic principle of restrainment is related to equation (1). The rectangular pulse of given amplitude and width is applied to the float when it is at a specified distance from zero, called the trigger level. The zero position corresponds

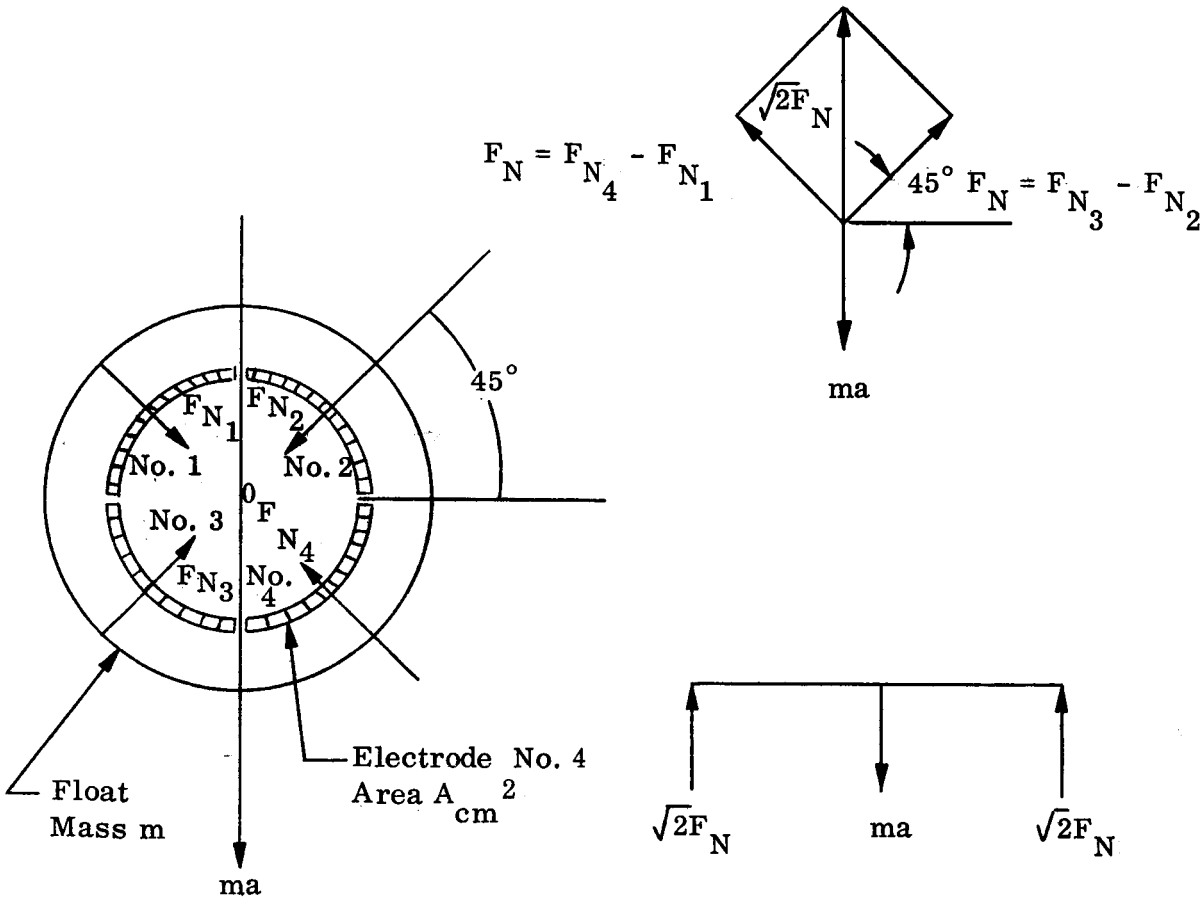

Figure 4. Equivalent Force Diagram of Suspension System

to a position of the float equidistant between the pickoff and/or forcer rings on either side of the float. Positive and negative pulses of equal amplitude and width are applied simultaneously to two forcer rings on the forcer block. They maintain the float at or near ground potential while attracting it in a direction opposite to that of the applied acceleration. With reference to Figure 5, the restoring force acting on the float is given by

$$F_P = K_f \left[\left(\frac{E_P^+}{d_1} \right)^2 + \left(\frac{E_P^-}{d_1} \right)^2 \right] \quad \text{dynes} \tag{12}$$

Defining $d_1 = \delta_f + x_f = \delta_f (1 + u_f)$, then

$$F_P = \frac{2K_f E_P^{\,2}}{\delta_f^{\,2} (1 + u_f)^2} \simeq \frac{2K_f E_P^{\,2} (1 - 2u_f)}{\delta_f^{\,2}} \quad \text{dynes} \tag{13}$$

where

K_f = 4.42×10^{-7}

A_f = forcer ring area cm^2

$u_f = \frac{x_f}{\delta_f}$ = normalized float displacement ($u_f << 1$)

δ_f = gap between forcer ring and flange on float when it is at its zero position

2.2.4 Analysis of Float Motion (Figure 6)

Consider a float with mass "m" under a total applied acceleration $\bar{a}$. The acceleration of the float is given by

$$\ddot{x} = \bar{a} - \xi \dot{x} \tag{14}$$

where

x = distance from an arbitrary zero position (cm)

$\bar{a}$ = total acceleration acting on the float (cm/sec^2)

a = acceleration to be measured (cm/ft^2)

ξ = damping constant (sec^{-1})

a_p = equivalent pulse acceleration (cm/sec^2)

$(\dot{})$ = differentiation with respect to time

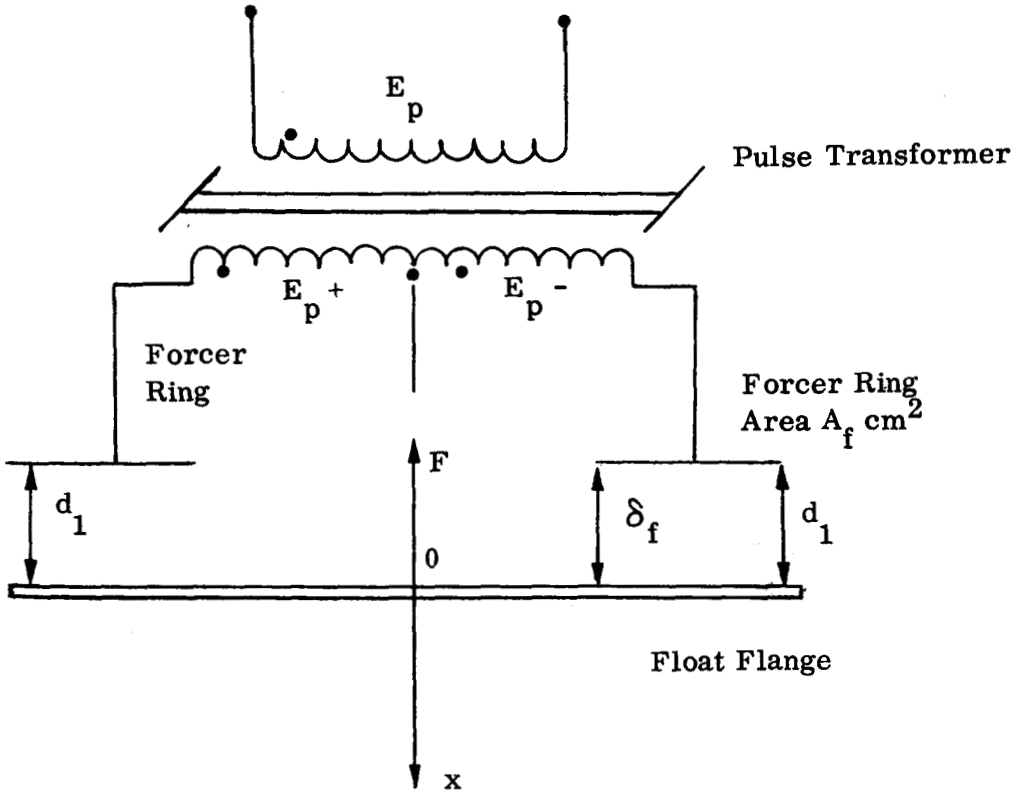

Figure 5. Restrainment System

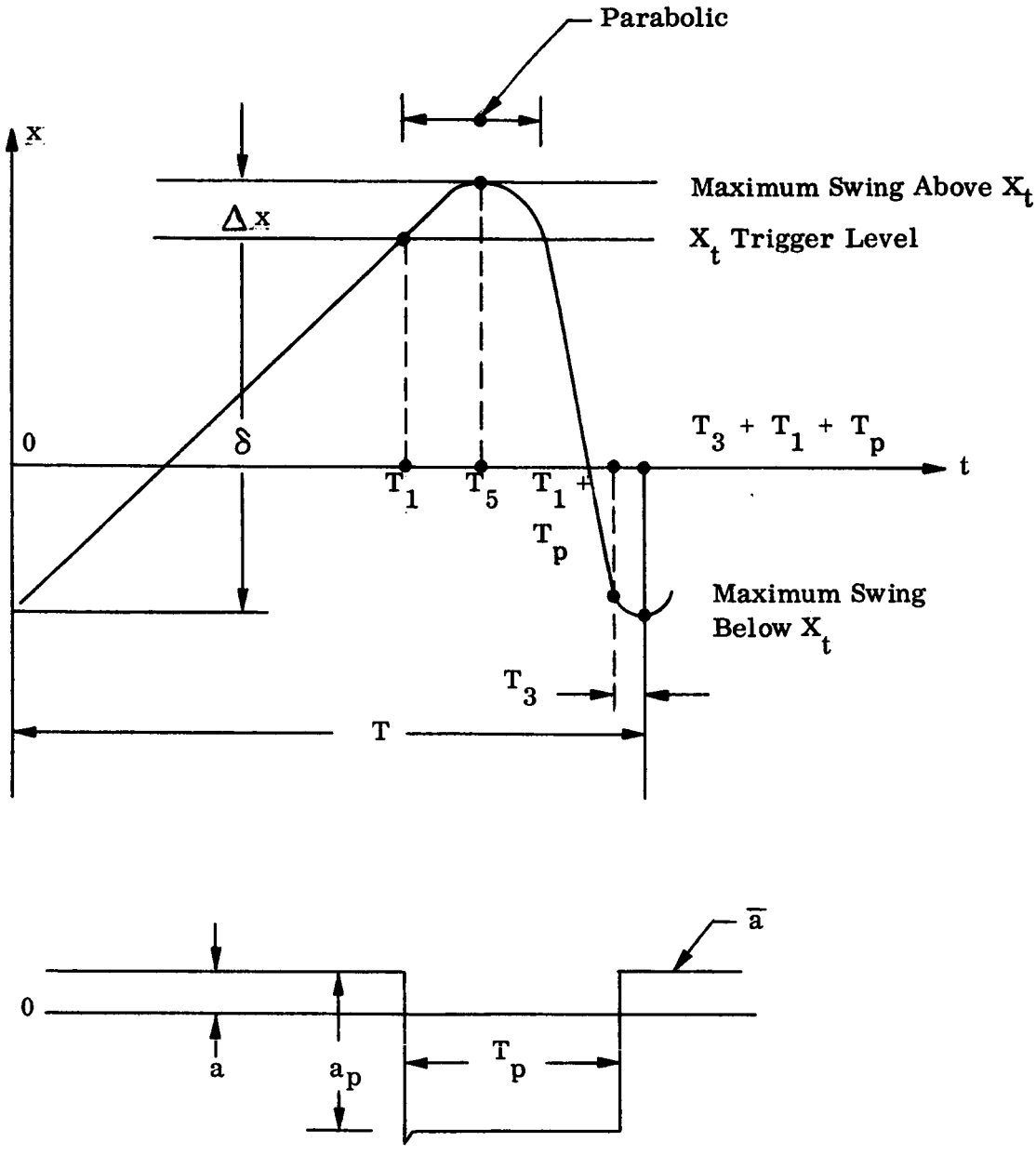

$\bar{a}$ = Total Acceleration Acting on Float

Figure 6. Float Motion

Equation (14) is integrated to find the velocity

$$\dot{x}(t) = \frac{\bar{a}}{\xi} + \left(\dot{x}(t_o) - \frac{\bar{a}}{\xi} \right) e^{-\xi (t - t_o)} \tag{15}$$

where

(t_o) = time when $\dot{x}(t) = 0$, $\bar{a} = a$

t_1 = start of pulse

t_p = length of pulse

t_3 = the time between the end of the pulse and the point where the float reaches its maximum excursion below the trigger level

By writing the expressions for $\dot{x}(t)$ at each of the various times and setting $x(t_1 + t_p + t_3) = 0$, it can be shown that

$$e^{\xi t_1} = \frac{a}{a_p} \frac{\left[e^{\frac{\xi t_p a_p}{a}} - 1 \right]}{\left[e^{\xi t_p} - 1 \right]} \tag{16}$$

This equation determines the time required to reach the trigger level from the maximum excursion of the float. Equation (15) is integrated to give the general distance formula.

$$x(t) = \frac{\bar{a}}{\xi^2} \left[\xi (t - t_o) + e^{-\xi (t - t_o)} - 1 \right] + \frac{\dot{x}(t_o)}{\xi} \left[1 - e^{-\xi (t - t_o)} \right] + x(t_o) \tag{17}$$

The equation of motion of the float may be written

$$m\ddot{x} + K_D \dot{x} = ma - F_p \tag{18}$$

where $\xi = \frac{K_D}{m}$ = damping constant = 2000 dynes/cm/sec (approx.)

F_p = force due to pulse

m = float mass = 0.72 gm

Substituting equation (13) for F_p,

$$\ddot{x} + \frac{K_D}{m}\dot{x} = a - \frac{2K_f E_p^2(t)}{m\delta_f^2}\left(1 - \frac{2x(t)}{\delta_f}\right) \tag{19}$$

Integrating equation (19),

$$\left[\dot{x}(t) - \dot{x}(0)\right] + \frac{K_D}{m}\left[x(t) - x(0)\right] = \int_0^t a\,dt - \frac{2K_f}{m\delta_f^2}\int_0^t E_p^2(t)\left(1 - \frac{2x(t)}{\delta_f}\right)dt \tag{20}$$

Assume

1. Motion is periodic with period T.
2. a is constant
3. $\int_0^t E_p^2(t)\,dt = \int_0^{t_p} E_p^2\,dt = E_p^2\,t_p$

   Pulse is rectangular with width T_p
4. $\int_0^t E_p^2(t)\frac{x(t)}{\delta_f}dt = \int_0^{t_p} E_p^2\,\frac{x(t_p)}{\delta_f}dt = E_p^2 t_p \frac{x_t}{\delta_f}$

where

x_T = trigger level distance

$\dot{x}(T) = \dot{x}(0)$ $\qquad$ $x(T) = x(0)$

$$\int_0^T a\,dt = \frac{2K_f}{m\delta_f^2} E_p^2 t_p \left(1 - \frac{2x_t}{\delta_f}\right) \tag{21}$$

$$aT = a_p t_p \tag{22}$$

where

$$a_p = \frac{2K_f E_p^2}{m\delta_f^2}\left(1 - \frac{2x_t}{\delta_f}\right) \text{cm/sec}^2 \tag{23}$$

$$f = \frac{1}{T} = \frac{a}{a_p t_p} \quad \text{cps} \tag{24}$$

Equation (24) expresses the basic principle upon which the digital accelerometer is based. The frequency of the float motion is proportional to acceleration, the number of pulses proportional to velocity. The proportionality constant is $a_p t_p$. Its stability and magnitude determine the scale factor stability and magnitude.

2.2.5 General Principle of Pickoff System (Figure 7)

The two pickoff rings form arms of a bridge which is balanced when the float is equidistant between each ring. This distance is referred to as the pickoff gap width δ_p. The bridge is excited by an a-c excitation voltage E_c which is amplitude modulated by the float movement. The bridge output at AB is amplified and then phase sensitive demodulated to provide a d-c signal proportional to the float position.

It may be shown that the output of the transformer when it is tuned to the excitation frequency f_o is

$$\frac{V_o}{E_c} = \frac{\omega_o C C_M R_L' u_p \quad \angle 90^\circ}{C + C_M} \tag{25}$$

where

u_p = normalized float displacement
C_M = pickoff centralized float capacity
C = bridge arm capacity
ω_o = $2\pi f_o$
R_L' = transformer tuned impedance in parallel with the load R_L on the transformer

Given f_o, E_c, R_L', C, and u_p the required pickoff capacity C_M may be determined for a given V_o.

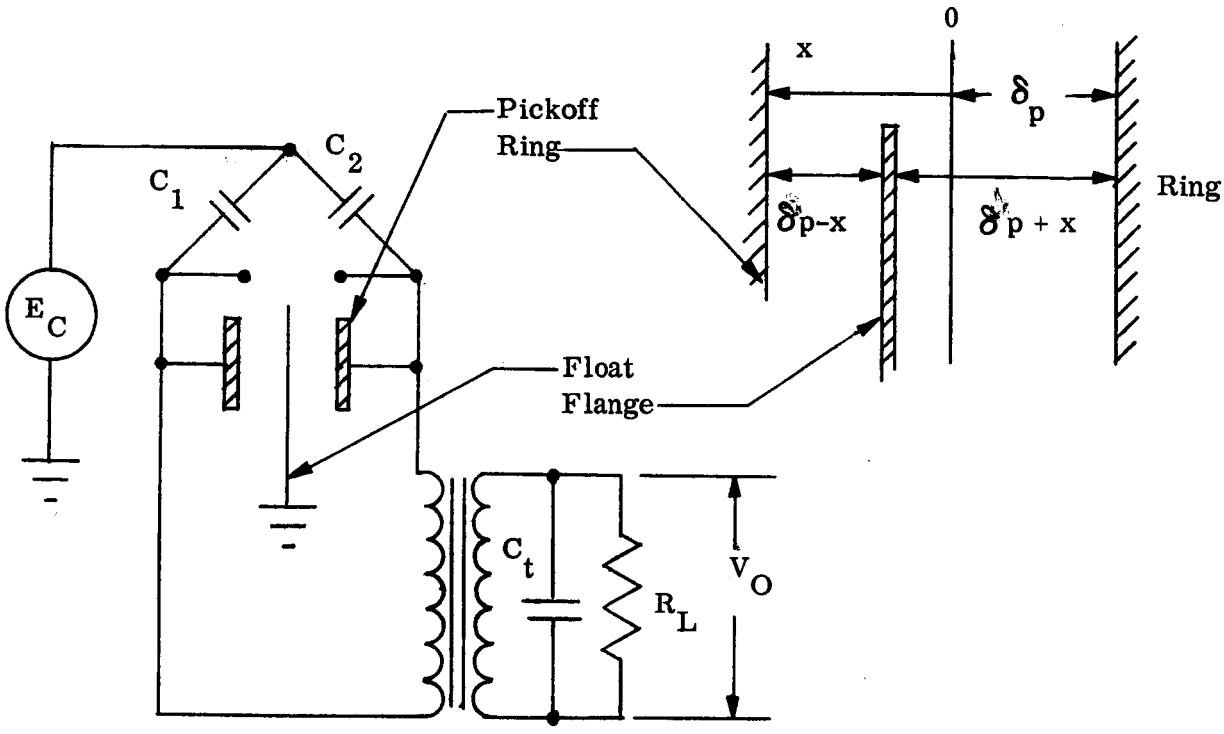

Tuned Transformer

Figure 7. Pickoff System

SECTION 3.0
MECHANICAL DESIGN

3.1 ACCELEROMETER

3.1.1 Float

One of the most difficult problems encountered in the accelerometer design was fabrication of the thin-walled beryllium float to very fine dimensional tolerances. Beryllium was used for its high strength-to-weight ratio and its good dimensional stability with temperature change. Cylinder straightness and roundness and flange flatness, parallelism and perpendicularity to the cylinder are rigidly controlled since they limit the cross-axis coupling coefficient of the instrument. Typical dimension are as follows (dimensions in inches):

Flange width	0.0150 ± 0.0005
Cylinder thickness	0.0050 ± 0.0002
Flange O.D.	1.282 ± 0.001
Cylinder I. D.	0.4991 ± 0.0002
Cylinder length	0.864 ± 0.001
Cylinder straightness and roundness	$< 10 \times 10^{-6}$
Flange squareness to cylinder diameter	< 0.0001
Surface finishes	$2 \text{ to } 10 \times 10^{-6}$ rms
Weight	0.72 gram

3.1.2 Electrode Carrier

The electrode carrier requirements impose relatively complex fabrication problems. The eight electrodes must be electrically conductive but well insulated from all others, and have a hard, smooth surface finish with no sharp corners or discontinuities. The assembly is fabricated with polished stainless steel electrodes embedded in high strength, low thermal coefficient, low dissipation, high resistivity

epoxy resin. Its O.D., electrode area, and surface finish are closely controlled to ensure good symmetry and force balance in the suspension system electric field. The carrier dimensions, in inches, are:

O.D.	0.496500 ± 0.000050
Length	1.220 nominal
Electrode length	0.339 ± 0.001
Straightness and roundness	$< 10 \times 10^{-6}$
Surface finish	$< 4 \times 10^{-6}$ rms

3.1.3 Forcer Block

The forcer block is an important element of the accelerometer design since it contains the pickoff and constrainment electrodes. It must have the same electrical properties as the electrode carrier including low stray capacity and high dimensional stability. Three concentric, equal area, stainless steel rings are embedded in epoxy resin. The inner and outer rings are forcer rings, energized by equal amplitude, opposite polarity constrainment pulses. They exert equal attractive forces on the float flange while inducing zero net charge on the float. The center ring is the pickoff ring, a fixed plate of the differential pickoff capacitor whose movable plate is the float flange. This ring geometry results in minimum interaction between the pickoff and forcer systems. Two forcer block assemblies on opposite sides of the float flange are used to achieve bidirectional constrainment and "balanced bridge" float motion detection. Typical dimensions, in inches, are:

O.D.	1.9300 ± 0.0001
Width	0.5917 ± 0.0005
I.D.	0.496300 ± 0.000050
Electrode rings	Flat within 5×10^{-6} TIR
Surface of rings	Perpendicular to O.D. within 10×10^{-6} TIR
Roundness of O.D. and I.D.	$< 50 \times 10^{-6}$ TIR

3.1.4 Bonnet and Inductor Terminal Boards

The pickoff bridge output is transformer coupled to an emitter follower stage for isolation from and impedance matching to the electronics interconnecting cable. The components are mounted on a terminal board at the connector end of the accelerometer (called the bonnet) within the housing.

The suspension electrodes (on the electrode carrier) and the float cylinder form the capacitors of the series tuned LC suspension circuits. The associated adjustable inductors and current limiting resistors are mounted on two terminal boards in sets of four "behind" each forcer block.

3.1.5 Housing

The aluminum housing, in conjunction with the forcer blocks and electrode carrier, determines the alignment between the float flange and the pickoff and forcer rings. The housing also establishes the accelerometer mounting surface and hence, sensitive axis alignment. All critical surfaces are polished to less than 10 micro-inches rms and parallelism and perpendicularity, where applicable, are maintained to 0.001 inch TIR. The assembled housing consists of top and bottom caps with O-ring seals to the center section.

3.1.6 The Accelerometer Assembly

Critical surfaces, including the exterior surface of the housing, are plated with an amorphous nickel-phosphorus coating (approximately 0.0003 in. thick) to provide solderable surfaces or to preclude aluminum to aluminum pressure fits. The uncoated surfaces were polished (where required) then the plating applied with negligible degradation of finish.

The O-ring sealed assembly is helium leak tested prior to the final fill with dry nitrogen at 1.0 atmosphere. The leak rate is verified to be less than 10^{-8} cc/sec. It is estimated that only 15% of the entrapped nitrogen would be lost per year at this average leak rate in a space environment.

The accelerometer is held at a constant operating temperature (approximately 35°C) by a wrap-around heater element in a thermistor-sensor temperature control loop. The stability of the internal temperature is better than ± 0.1°C over the anticipated operating range of 25 ±5°C. Thermal isolation from its mounting surface is achieved by use of a mounting ring of dense, rigid ceramoplastic material with excellent dimensional stability and very high dielectric strength (called Mykroy).

3.2 ELECTRONICS ASSEMBLY

The electronics package contains all the subsystems for power conditioning, output signal generation and suspension, constrainment, and pickoff electronics. The subsystems are constructed of welded or soldered cordwood modules fastened to fiberglass "mother" boards. Selected components for circuit adjustment and trimming are mounted on these boards. Intercircuit wiring is arranged to allow easy access to all circuits by folding top boards out to reach lower level circuits. All suspension and pickoff circuit screwdriver adjustments are available by removing the main cover only. The pulse generation circuits and their associated vernier temperature controllers are placed in an oven occupying one end of the assembly.

The package is attached to its mounting base by five pads to ensure structural rigidity while minimizing heat transfer to the environment.

SECTION 4.0
ELECTRICAL DESIGN

4.1 SUSPENSION SYSTEM

The eight tuned circuits which make up the accelerometer suspension are supplied by a balanced a-c voltage from a transformer-coupled amplifier. Balancing is achieved by a potentiometer-capacitor combination at the amplifier output to adjust the sum of the suspension line currents to zero. The system is designed for automatic suspension of the proof mass without arcing or voltage breakdown. The suspension voltage amplitude is adjustable and determined by the accelerometer cross-axis g load.

4.1.1 Suspension Oscillator

The suspension oscillator provides a variable frequency signal which sweeps smoothly from approximately 1.4 to 1.100 mcps in approximately five seconds to produce float liftoff and suspension. By changing the excitation frequency in this manner, the voltage gradient across the electrode-float gap builds up gradually and minimizes the possibility of voltage breakdown. Noninstantaneous operating frequency change is necessary also to maintain a stable relationship between the individual tuned circuit resonant frequency shifts (produced by the respective electrode-float capacity changes during liftoff) and the excitation frequency. Float inertia and damping limit the minimum stable sweep time to approximately 0.5 second.

The oscillator is a conventional tuned collector LC oscillator with voltage variable capacitors in the tank circuit which produce a frequency change proportional to an impressed d-c voltage. When at the REST (float not suspended) frequency, 24 vdc is applied to the CONTROL terminal to produce an excitation frequency of approximately 1.4 mcps. To start the sweepdown, the 24 vdc is removed. The voltage across the varicap diodes decreases along an exponential curve established by an RC timing network resulting in a decreasing oscillator frequency. When the

operating frequency of 1.100 mcps is reached, a regulator circuit consisting of a 1.100 mcps crystal and a voltage doubler causes the sweep action to cease. A portion of the oscillator output voltage is coupled to the voltage doubler through the crystal. The doubler output is added to the decaying varicap voltage through a diode. When the sweeping frequency reaches the crystal resonant frequency, the doubler output rises sharply (due to crystal Q) to the varicap voltage necessary to maintain the crystal resonant frequency. This is called the FLOAT (suspended) frequency. Resetting to the REST frequency may be done instantaneously without damage to the float.

4.1.2 Suspension Amplifier

The suspension amplifier is a wideband feedback type which amplifies the sweep oscillator output. The amplifier output is transformer-coupled to the eight tuned circuits along two output lines which are balanced to ground; amplitude-wise by a potentiometer across them with its arm grounded, and phase-wise by a selected fixed capacitor to balance line capacity to ground. The nominal closed loop gain is 15 with stability of 1%. Its output impedance is less than 20 ohms to assure high tuned circuit Q. The output level is adjustable by a potentiometer at its input.

4.2 PICKOFF SYSTEM

The pickoff system (Figure 8) is the amplitude-modulated suppressed-carrier type. Float movement along its sensitive axis produces an amplitude-modulated 192 kc signal at the bridge output. This signal is filtered, amplified and phase demodulated. The result is a d-c signal whose amplitude is a measure of float displacement and whose polarity indicates direction of motion. Typical pickoff loop gain is 60,000 v/cm at the demodulator output.

4.2.1 Capacitive Bridge and Buffer (Bonnet Electronics)

The fixed arms of the capacitive pickoff bridge are stable ceramic capacitors, the differential arms are the float-ring combination. The bridge output signal is coupled through a double shielded transformer to an emitter-follower buffer stage. A degree of filtering is obtained by tuning the transformer secondary to the carrier frequency, 192 kc.

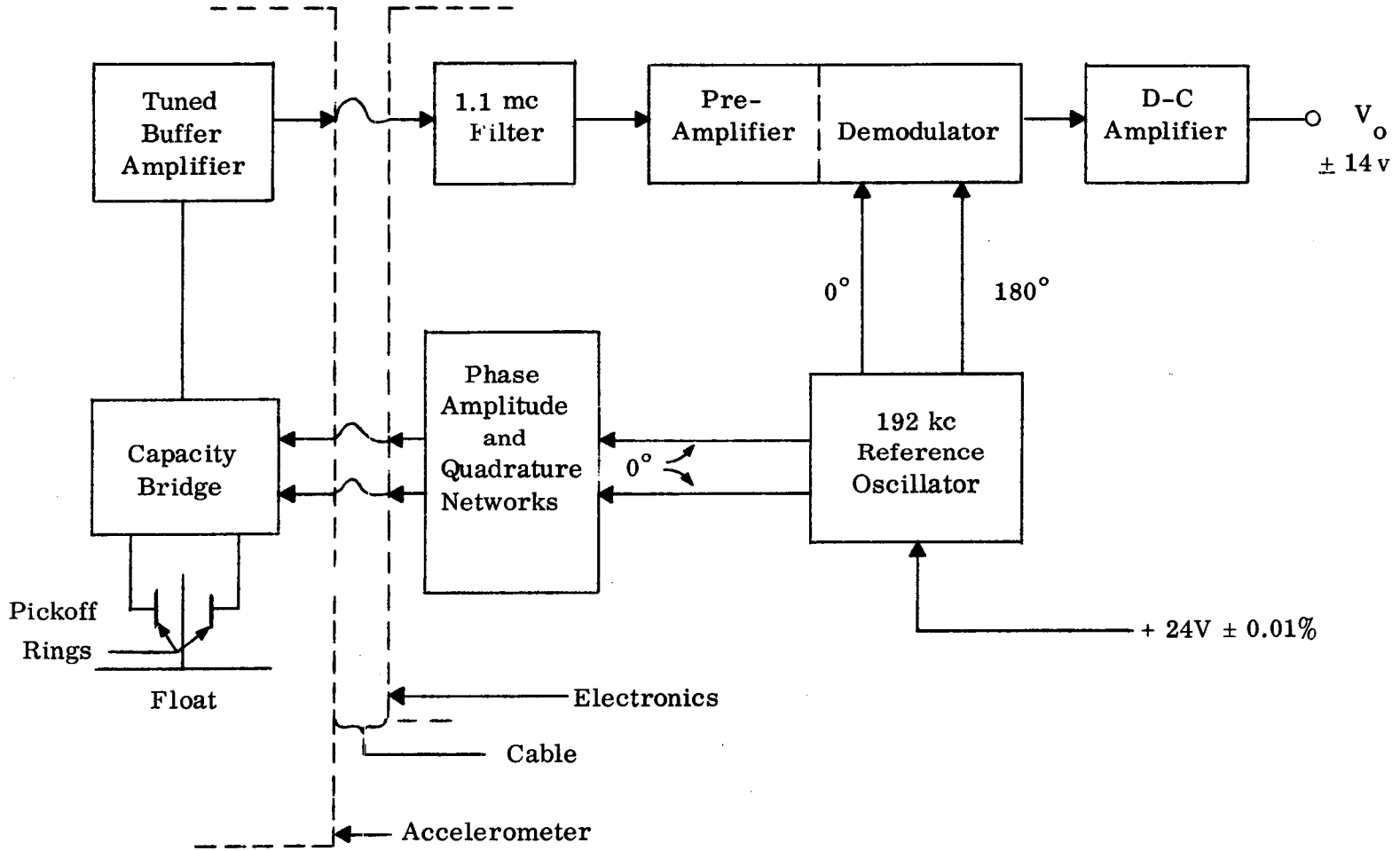

Figure 8. Pickoff System

4.2.2 1.1 mc Filter

The "bonnet" output signal passes through a 1.1 mc trap which suppresses unwanted pickup from suspension system wiring by 30 db.

4.2.3 Preamplifier/Demodulator

The preamplifier section of this module provides an a-c gain of 50 at 192 kcps. It is a feedback amplifier with transformer coupled output to the demodulator section and has gain stability of 1.5%. The demodulator is a full-wave bridge rectifier type deriving its reference voltage from the 192 kc reference oscillator.

4.2.4 D-C Amplifier

The d-c amplifier is a conventional design with its closed-loop gain adjusted to approximately 30. Cascaded differential amplifiers are used in the first two stages (feeding a single-ended output stage) to obtain good thermal stability without exotic compensation. At its input are a 384 kc trap to suppress the demodulator output ripple and a 30 kc rolloff network to attenuate high frequency noise. Its output voltage range is zero to ±14 vdc.

4.2.5 192 kc Reference Oscillator

The reference oscillator is a crystal controlled Colpitts type circuit. The output is regulated by a Zener diode limiter, followed by the tuned output transformer. Two isolated output windings supply the reference voltage to the demodulator section of the preamplifier/demod and the accelerometer bridge excitation voltage through the phase, amplitude and quadrature networks.

4.2.6 Phase, Amplitude and Quadrature Networks

A high resolution, low resistance potentiometer between the upper fixed bridge capacitors allows equalization of impedances between the two sides of the bridge, thereby minimizing quadrature content in the bridge output signal. An RC constant amplitude phase shift network across the reference oscillator centertapped winding is used to compensate for phase shifts between the demodulator input and

reference voltages to minimize the magnitude of carrier signal in the d-c null. A potentiometer at the phase shifter output allows optimum adjustment of pickoff loop gain by controlling the bridge excitation voltage. Each of these adjustments is easily accessible on terminal boards.

4.3 PULSE GENERATION SYSTEM

One of the most critical performance parameters is the stability of the forcer pulse size. The method of generation and control of pulses is to switch a saturable core transformer between its two saturated states while maintaining its magnetic parameters constant by extremely tight temperature control of its tape wound core and good regulation of its supply voltage. The MESA system (Figure 9) employs two identical channels each feeding a set of accelerometer forcer rings.

4.3.1 ±Trigger Circuit

The ± trigger circuit is a dual channel level sensor set to deliver a turn-on signal to the positive pulse generator when its input voltage reaches +7 volts and to the negative generator for -7 volt input. The actuating signal remains until the float motion input voltage has been reduced below the respective trigger level by the forcer pulses thus applied. The turn-on signals are produced when the float motion voltage exceeds the conduction levels of oppositely oriented Zener diodes (approximately 7 volt types).

4.3.2 Multivibrators

Identical multivibrators are used in the (+) and (-) channels. They consist of a latching stage, which is "unlatched" by the proper turn-on signal from the ± trigger; followed by a free-running multivibrator adjusted to a free-running rate of 5 kcps; and a flip-flop triggered from the multivibrator to control the core switching transistors.

The latching stage receives a "hold" or set signal from the multivibrator to prevent relatching during a pulse interval. Therefore, the circuit gates only integral numbers of pulses to the forcer rings. The minimum pulse spacing (200

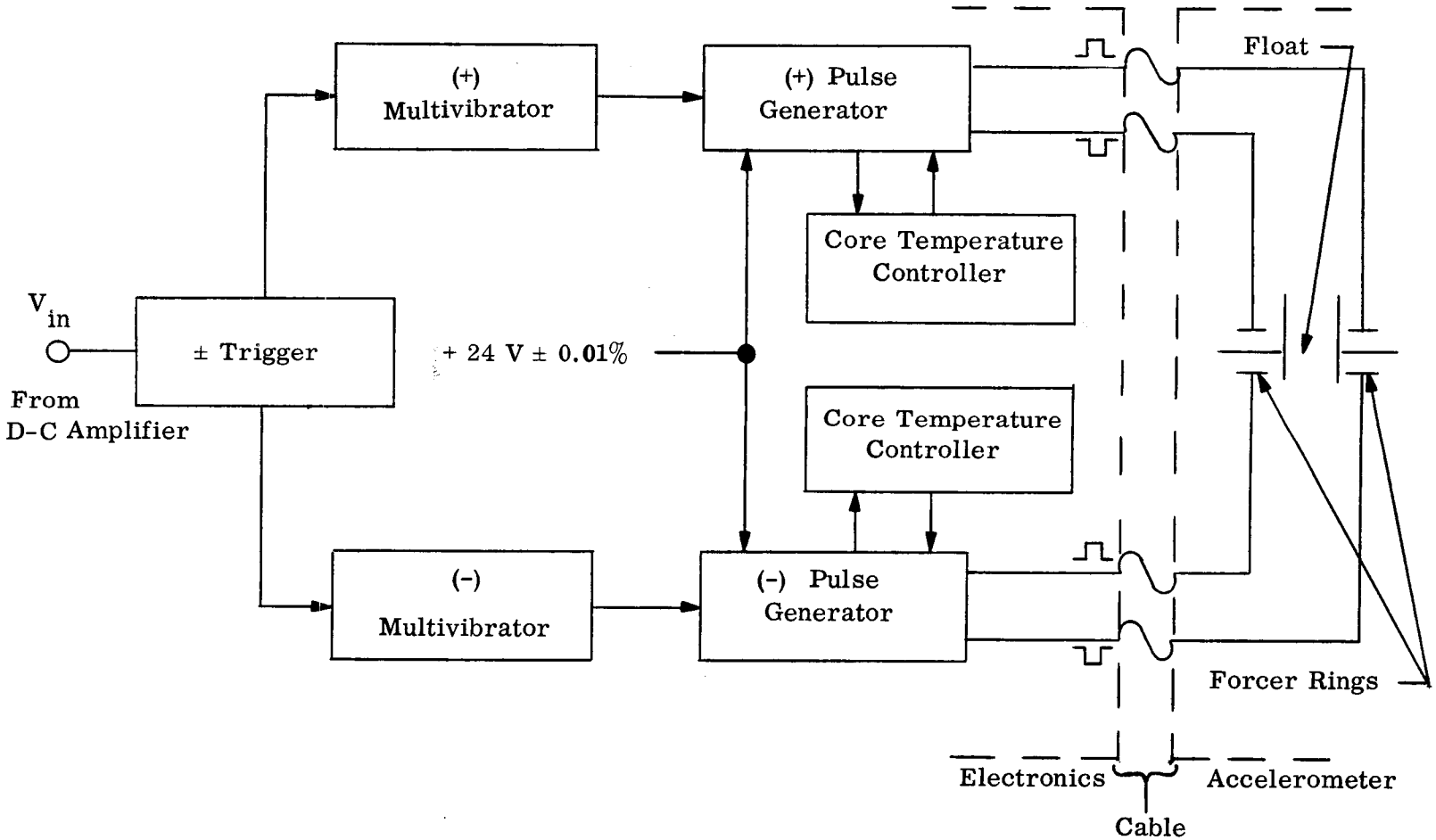

Figure 9. Pulse Generation System

microseconds) is also established by the free-running multivibrator to prevent the pulses from running too close together. Digital output pulses are also generated by this circuit.

4.3.3 Pulse Generators

The pulse transformer, a saturable tape-wound core type, has a center-tapped primary which is switched alternately by transistors driven by the multivibrator. The secondary is tapped for approximately 300, 10, and 3 volts (peak) for 1, 10^{-3} and 10^{-4} g constrainment, respectively. Nominal pulsewidth is 160 microseconds. The primary supply voltage is nominally 24 vdc, regulated to 0.02% or better through a ±20 ppm/°C limiting resistor to maintain stable magnetization current.

4.3.4 Core Temperature Control

The stability of the pulse generator is determined by several factors, one being the temperature variation of the magnetic tape in the pulse transformer. To control the tape temperature to ±0.05°C with changes in external ambient and internal power dissipation, the resistance of the tape is sensed in a d-c bridge circuit. Any variation in tape resistance due to temperature change produces a bridge error signal which is d-c amplified. This voltage controls a duty cycle modulated a-c to d-c converter which controls the d-c current through the bridge. This current passes through the tape and controls its temperature by varying its power dissipation. This circuit is compensated also for the magnetostrictive effect which produces a tape resistance change during the interval a pulse is being generated. The uncompensated effect produces a scale factor nonlinearity of increasing degree as pulse rate increases.

4.4 MISCELLANEOUS ELECTRONICS

4.4.1 Temperature Controls

The temperature control electronics for the electronics assembly oven and the accelerometer are identical. Each employs thermistor sensors in the controlled region, d-c bridge error sensing, d-c amplification and proportional control

of the heater elements. Each is capable of 1°C control for an ambient variation of 50°C.

4.4.2 Power Supply

All operating power is derived from a single 28 vdc supply. Power conditioning is accomplished by a simple, sure-start multivibrator d-c to a-c converter which switches the centertapped primary of a power transformer wound with appropriate secondaries for producing rectified and filtered d-c voltages at +28, -16 and 6 volts (two isolated supplies).

4.4.3 Precision Regulator

Stable voltage for pulse generator transformer primaries and B+ for the suspension oscillator, 192 kc reference oscillator, and core temperature controls is supplied by a conventional Zener regulated, series controlled voltage regulator operating from the raw 28 vdc from the power supply. Stability with line, load, and temperature changes is ±0.01%.

SECTION 5.0

SYSTEM TEST

The primary objective of tests conducted on the MESA were to show that its performance meets or exceeds the specification requirements. The following tests were conducted to verify, within the limits of the test instrumentation, MESA performance characteristics.

5.1 NULL

The objectives of this test were to measure:

(1) Null bias

(2) Long term null stability

(3) Null temperature sensitivity

5.1.1 Null Bias

Since the instrument sensitive and cross-axes cannot be made exactly orthogonal, some coupling of the suspension force into sensitive axis occurs. In the MESA, this is predominantly caused by the taper and out-of-roundness of the float cylinder. In order to achieve minimum cross-coupling, the thin-walled beryllium cylinder must be both round and straight to within 10 micro-inches.

The measured null bias for a 1 g suspension was -1.3×10^{-4} g for accelerometer SN 101 and -3.9×10^{-4} g for SN 102. These values can be expected to be reduced by a factor of 10 with improved machining and measurement techniques.

5.1.2 Long Term Null Stability

Although null bias is an important error source, its stability is of more importance. The null bias may be calibrated in any acceleration measurement. However, if the bias is not stable, accuracy of acceleration measurement is directly limited by the bias stability.

Null stability measurements were conducted with a 10^{-4} g input and the variations automatically recorded for running periods of up to 12 hours. Figures 10, 13, and 16, show peak to peak null variations of less than 1×10^{-6} g for SN 101 and SN 102.

It should be noted that test stand tilt variations cannot be readily distinguished from null variations. As is shown in the section following on scale factor stability, the same order of magnitude variations occur. It may be concluded that the ultimate null and scale factor stability of the MESA are better than or equal to the test base stability.

5.1.3 Null Temperature Sensitivity

The null varies with both accelerometer and electronics temperature changes. This is due to suspension excitation amplitude change and float-electrode carrier gap width changes. For a 1 g suspension, values of -2×10^{-7} and $+3.2 \times 10^{-6}$ g/°F/g were obtained for electronics and accelerometer (SN 101) temperature changes, respectively. A coefficient of $+1.18 \times 10^{-6}$ g/°F/g was obtained on accelerometer SN 102. These low values illustrate the high performance of the electrostatic suspension system.

5.2 SCALE FACTOR

The objectives of these tests were to adjust or measure:

(1) Channel balance

(2) Long term scale factor stability

(3) Scale factor temperature sensitivity

(4) Scale factor linearity

5.2.1 Channel Balance

The MESA system utilizes separate but identical constrainment pulse generation channels to supply the two sets of accelerometer forcer rings. Differences in forcer ring area and pulse transformer characteristics require compensation to the positive and negative scale factors. This balance is achieved by adjusting the

pickoff bridge balance position (the electrical null) to coincide with the position of equal pulse force (the mechanical null). Channel balance is accomplished by selection of value and position of capacitors 1A5C10,-C11, and -C12. It was set to 0.7% with accelerometer SN 101 and to 0.9% with SN 102.

5.2.2 Long Term Scale Factor Stability

The effect of test base on null tests mentioned in Section 5.1.2 is also a factor in scale factor stability measurement. Scale factor stability is also dependent on the stabilities of pulse transformer saturation current (which is determined by B+ and series resistor) and pulse transformer core temperature.

Scale factor measurements were made with 10^{-3} g (full scale) inputs over 8 to 12 hour periods. Figures 11, 12, 14, 15, 17, and 18 show peak to peak variations of less than 8×10^{-7} g for SN 101 and 1.5×10^{-6} g for SN 102.

5.2.3 Scale Factor Temperature Sensitivity

Tests were conducted on the electronics and the accelerometer to evaluate scale factor temperature sensitivities. The following data was obtained:

Electronics	$+3.5 \times 10^{-7}$ g/°F
Accelerometer	SN 101 $\leq +7.8 \times 10^{-7}$ g/°F
Accelerometer	SN 102 $\leq +6.8 \times 10^{-7}$ g/°F

5.2.4 Scale Factor Linearity

Scale factor linearity error is primarily caused by variation in pulse size with pulse rate, and is minimized by controlling the pulse core temperature. The tests conducted on the system level are limited by the accuracy of the resolution and stability of the g input to the accelerometer. Since this is typically 10^{-5} g, the linearity error coefficient would be 10^{-2} g/g at 10^{-3} g input and 10^{-1} g/g at 10^{-4} g input. A coefficient of less than 10^{-2} g/g, which is within the instrumentation error, was obtained in the tests on the system.

In order to check pulse size variation with frequency more accurately, the pulse generation system was tested in an analog to digital converter. The pulses

were compared with a precision d-c (10 ppm) voltage standard. The maximum linearity error measured was 0.05%.

5.3 SHOCK AND VIBRATION TESTS

The system was subjected to the shock and vibration tests shown in Figure 19. Subsequent post environment test indicated no measurable change in scale factor or null or failure in subsystem operation. Post environmental null and scale factor stability test data is shown in Figures 16, 17, and 18.

5.4 ERROR ANALYSIS

An acceleration measurement accuracy of ±1% or $\pm 3 \times 10^{-8}$ g, whichever is greater, is required for accelerations from 10^{-4} g to 10^{-6} g. The system error sources are:

(1) Scale factor stability E_k $\qquad E_t = \sqrt{E_k^2 + E_n^2 + E_L^2}$

(2) Null and null stability E_n

(3) Scale factor linearity E_L

The allowable rms error for each of the above sources is

$$E_k = E_n = E_L = 0.58\%$$

Where E_t = total system error

5.4.1 Scale Factor Stability

As shown in Figures 11, 12, 14, 15, 17, and 18 and as discussed in Section 5.2.2, the long term scale factor stability variations were less than 1.5×10^{-6} g peak to peak and the percent error less than 0.15%, a factor of four better than the requirement. The scale factor temperature coefficient is 1.1×10^{-6} g/°F or 0.11%/°F. For a ±5°C environment, the error contribution by the electronics is ±0.31%; and by the accelerometer, which is temperature controlled to ±2°F, is ±0.16%.

5.4.2 Null and Null Stability

The allowable null error for a 10^{-4} g input is 5.8×10^{-7} g. For a 10^{-6} g input, the allowable system error is 3×10^{-8} g, which is also the null error in this

case since the scale factor errors are less than 5.8×10^{-9} g. The typical null bias is 10^{-4} g/g, which for 10^{-4} g cross-axis suspension is 10^{-8} g. The system worst case null temperature coefficient is 3×10^{-6} g/g/°F, the error being 6×10^{-10} g/°F for a 10^{-4} g suspension and 2°F temperature control of the accelerometer. The long term null variation was 10^{-6} g peak to peak for a 1 g suspension, and would be in the order of 10^{-10} g for a 10^{-4} g suspension.

5.4.3 Scale Factor Linearity

The allowable linearity error is 5.8×10^{-3} g/g. As discussed in Section 5.2.4, the tests on a system level cannot be made to this accuracy. In the subsystem test of the pulse generation system, the maximum error was 0.05% or 5×10^{-4} g/g.

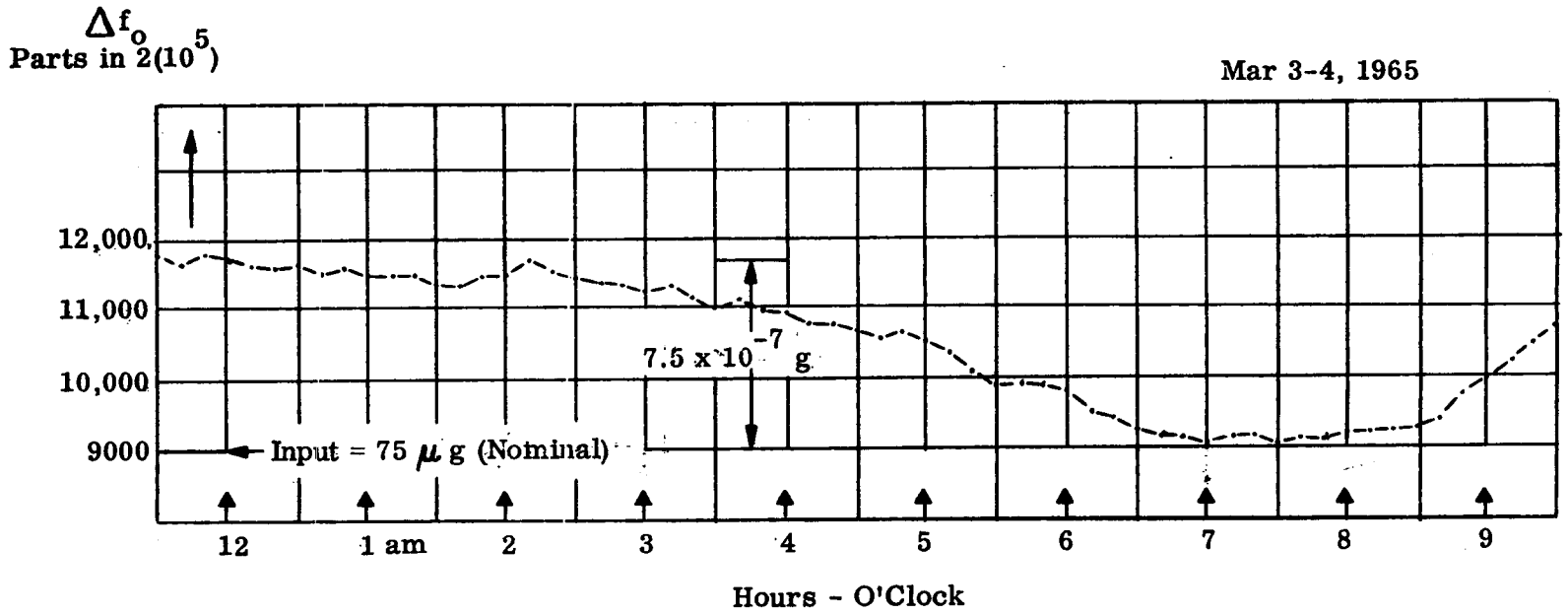

Figure 10. Null Stability; SN 101 Before Environmental Tests

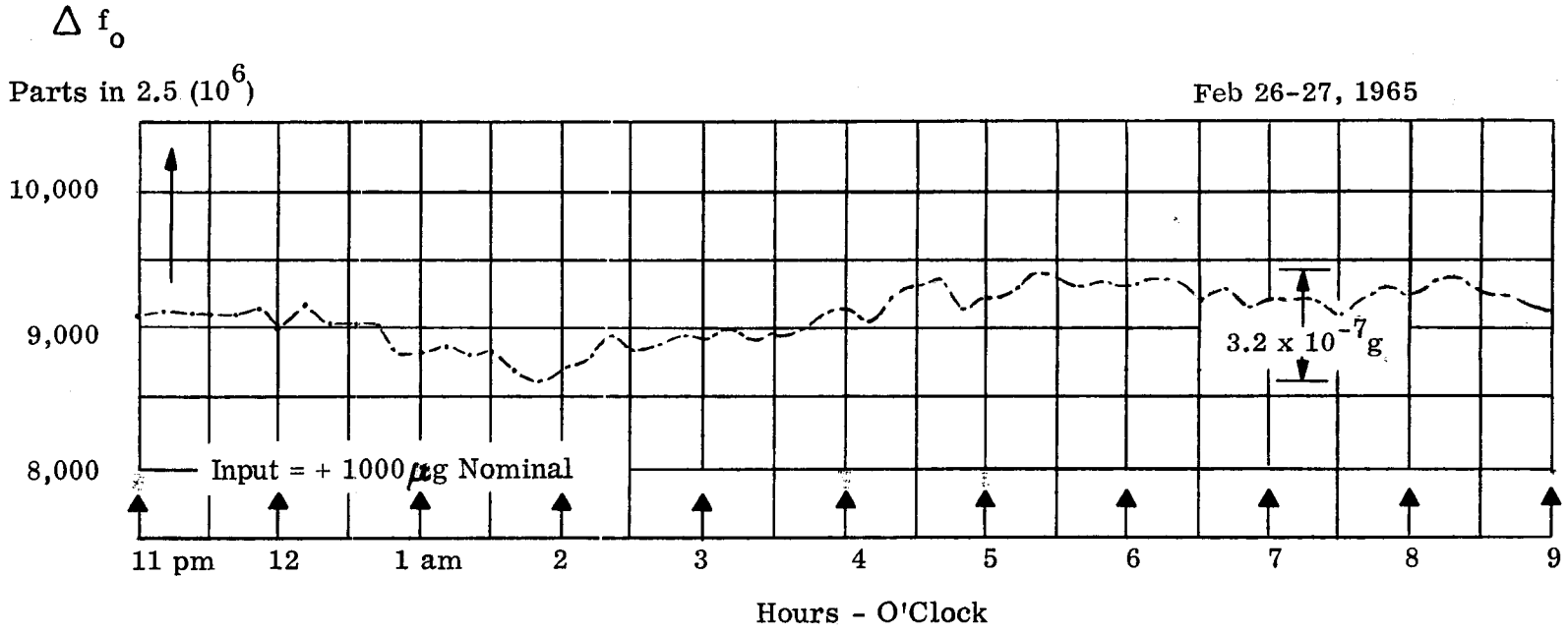

Figure 11. Scale Factor Stability; SN 101 Before Environmental Tests

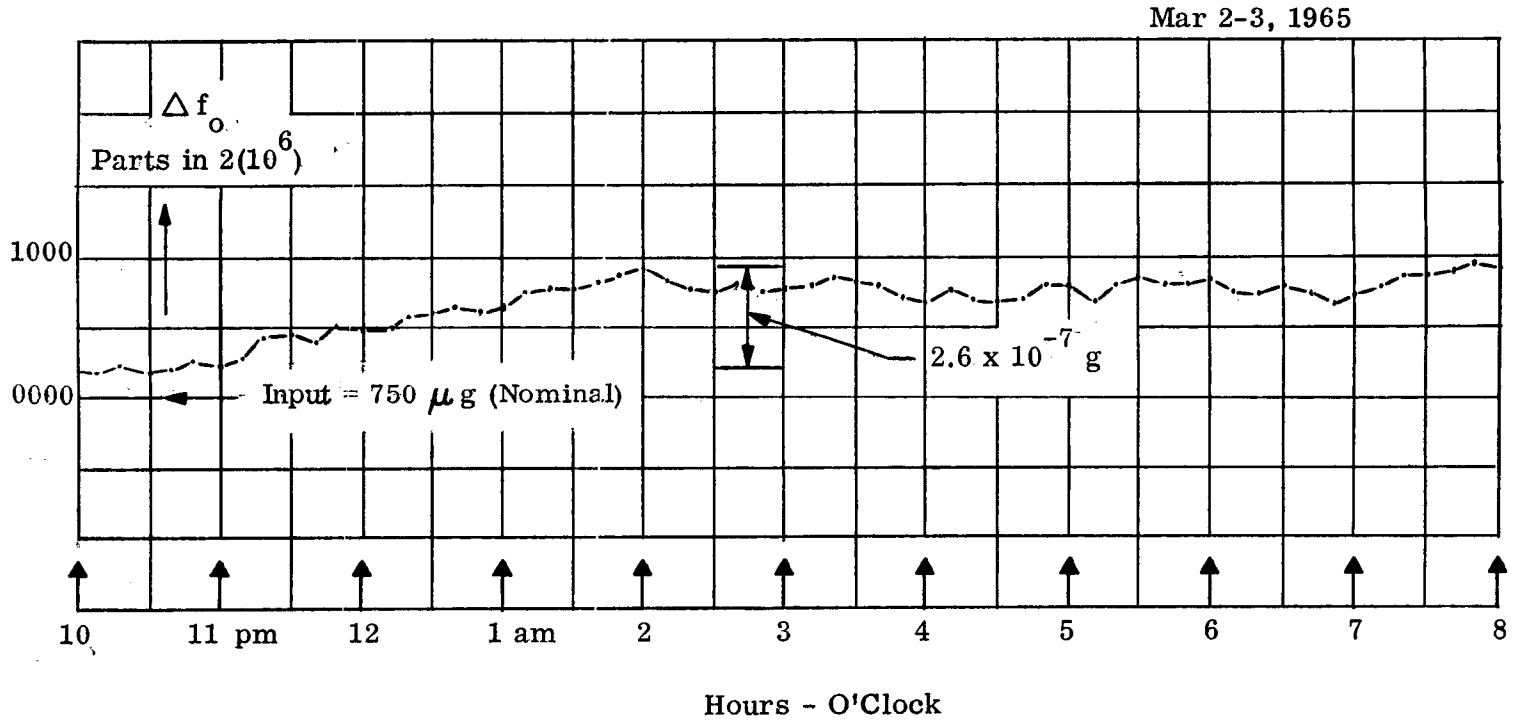

Figure 12. Scale Factor Stability; SN 101 Before Environmental Tests

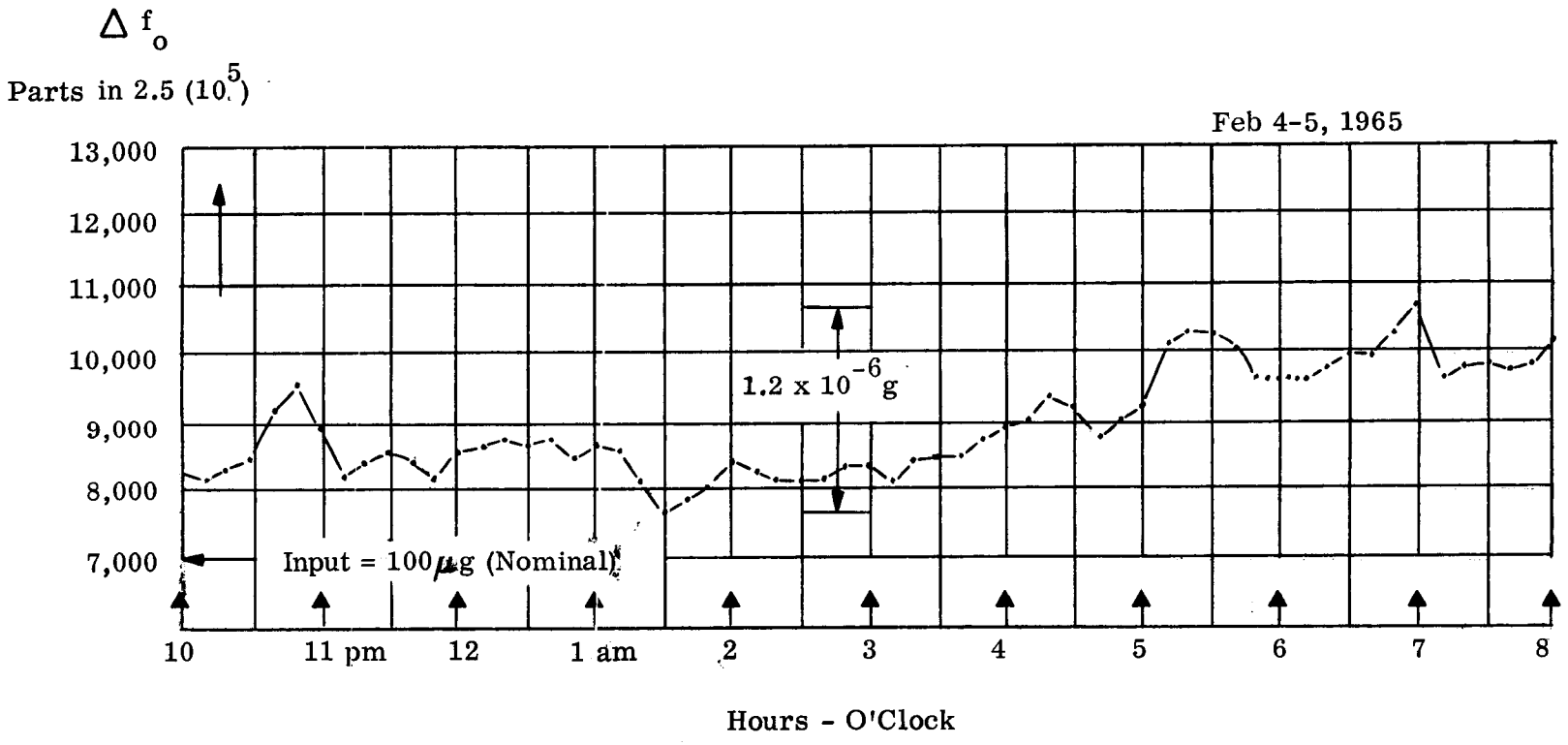

Figure 13. Null Stability; SN 102 Before Environmental Tests

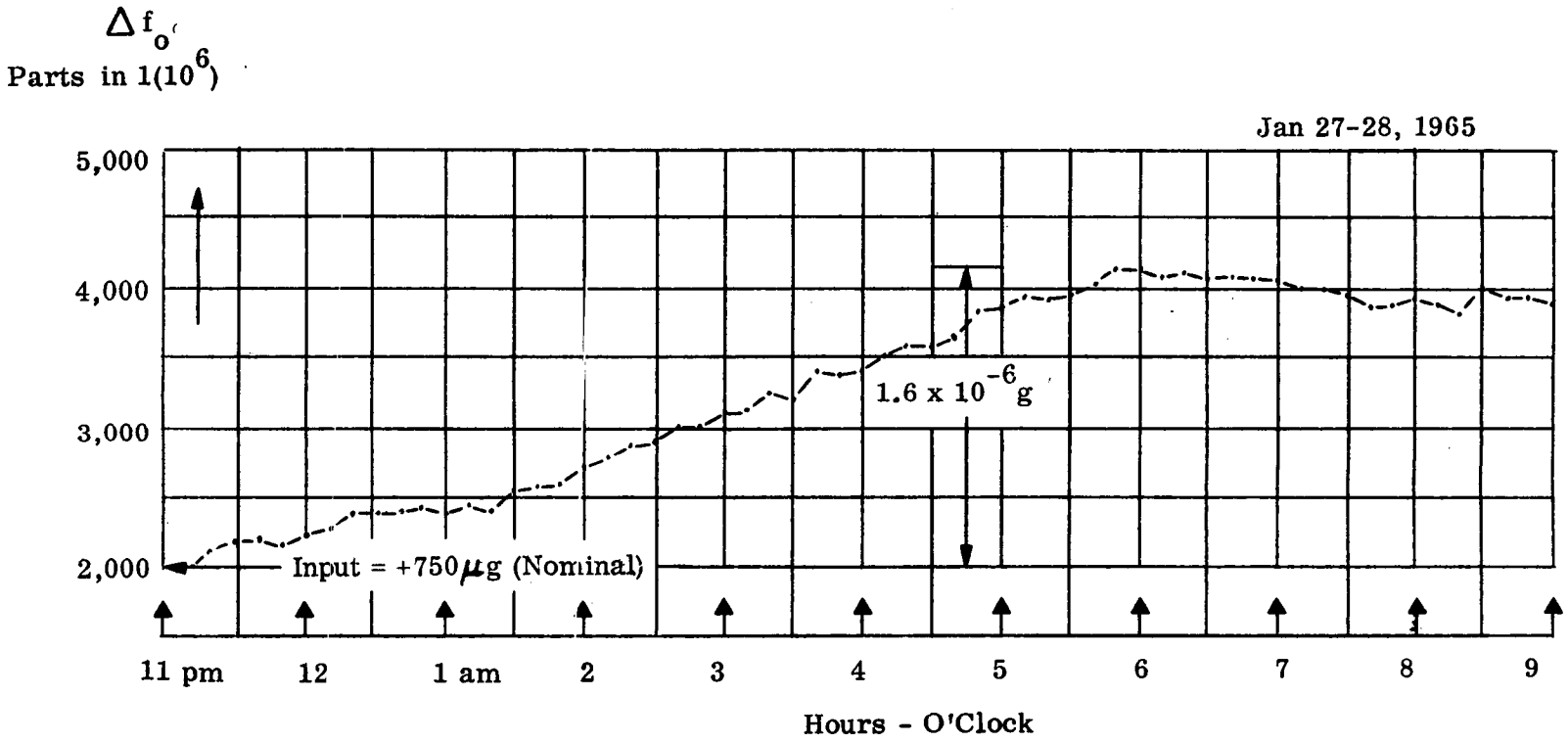

Figure 14. Scale Factor Stability; SN 102 Before Environmental Tests

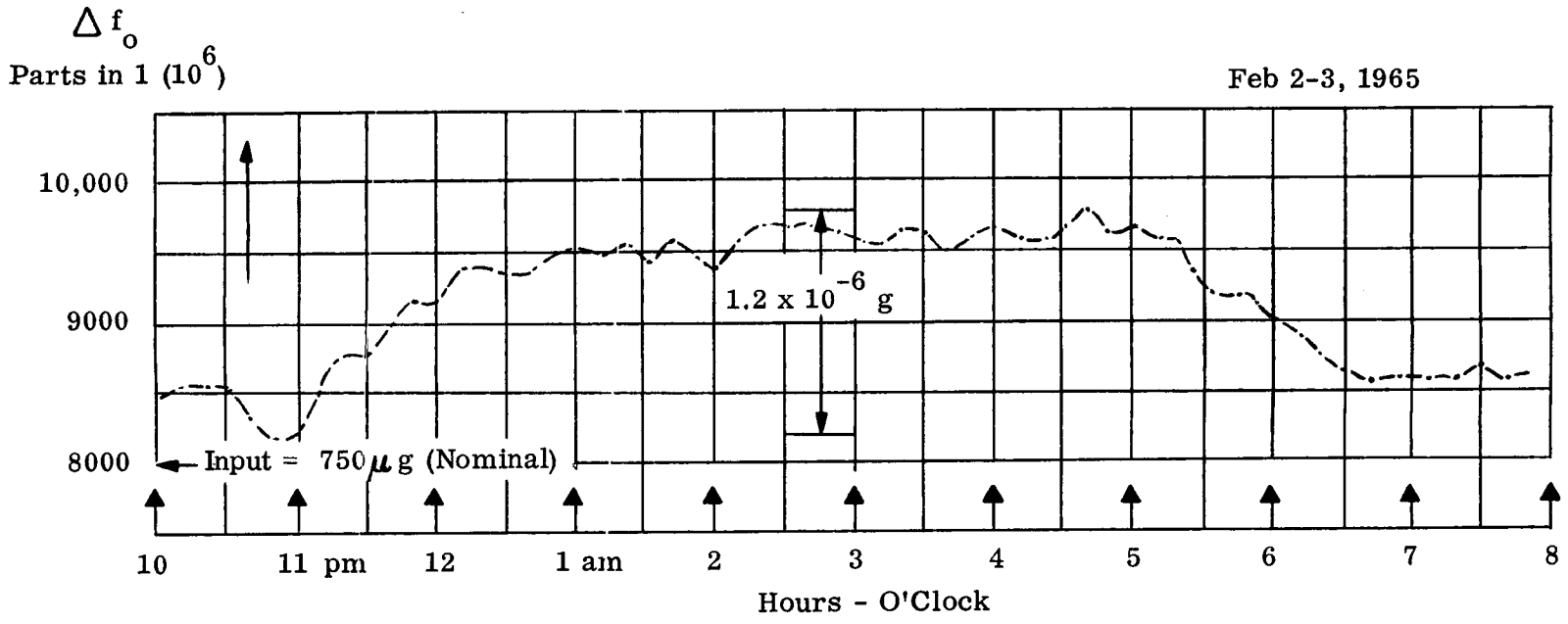

Figure 15. Scale Factor Stability; SN 102 Before Environmental Tests

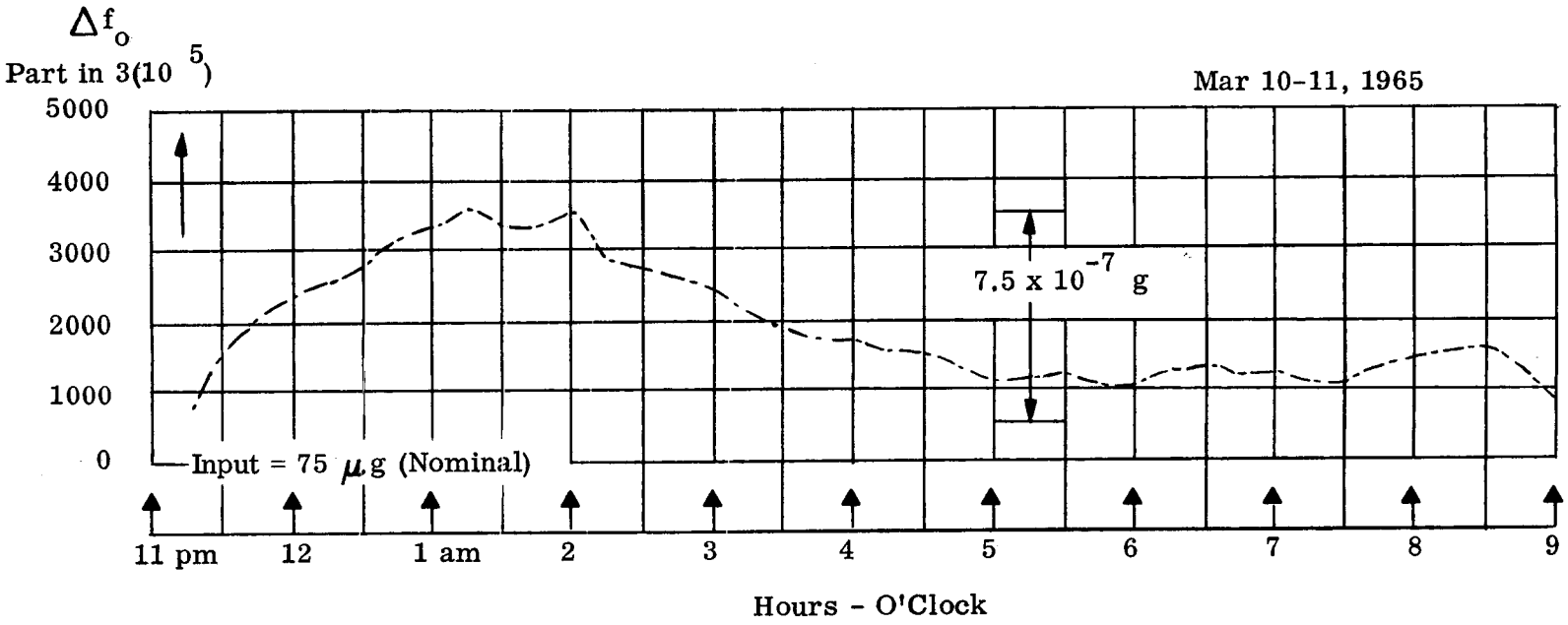

Figure 16. Null Stability; SN 101 After Environmental Tests

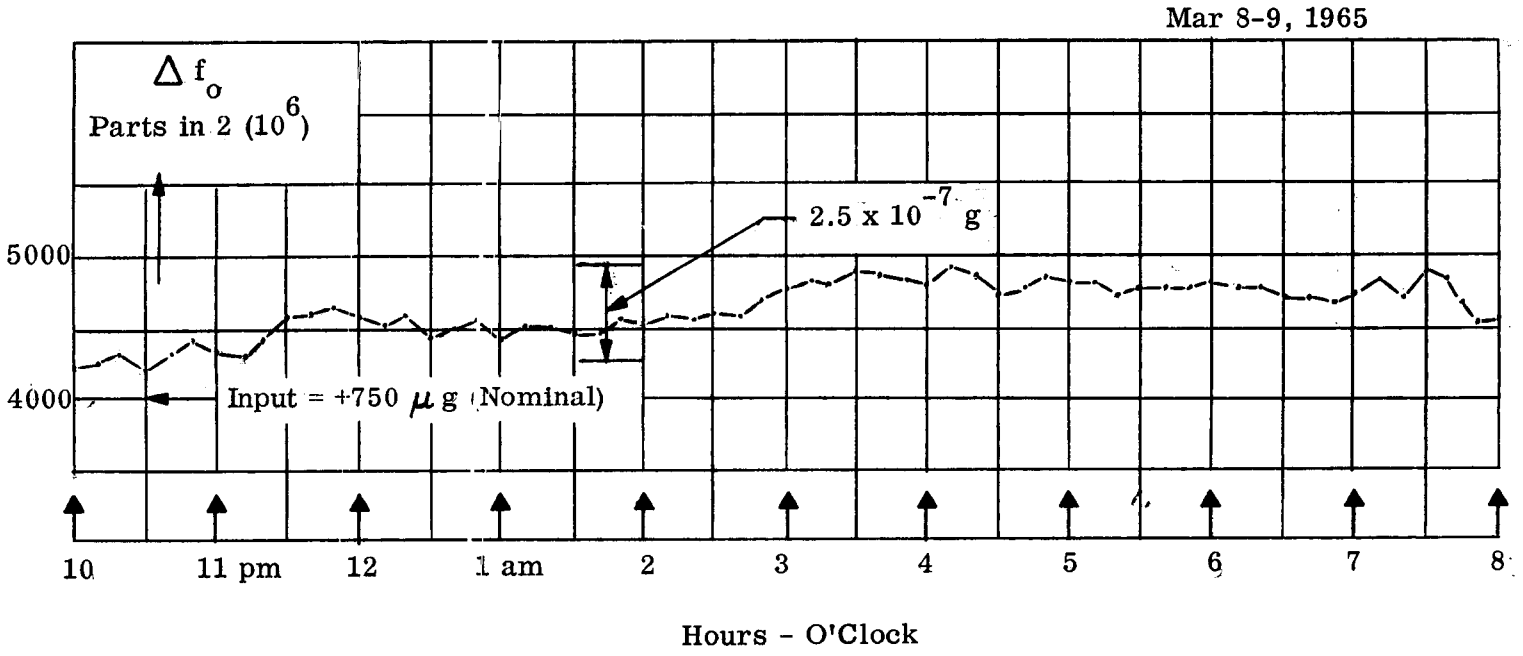

Figure 17. Scale Factor Stability; SN 101 After Environmental Tests

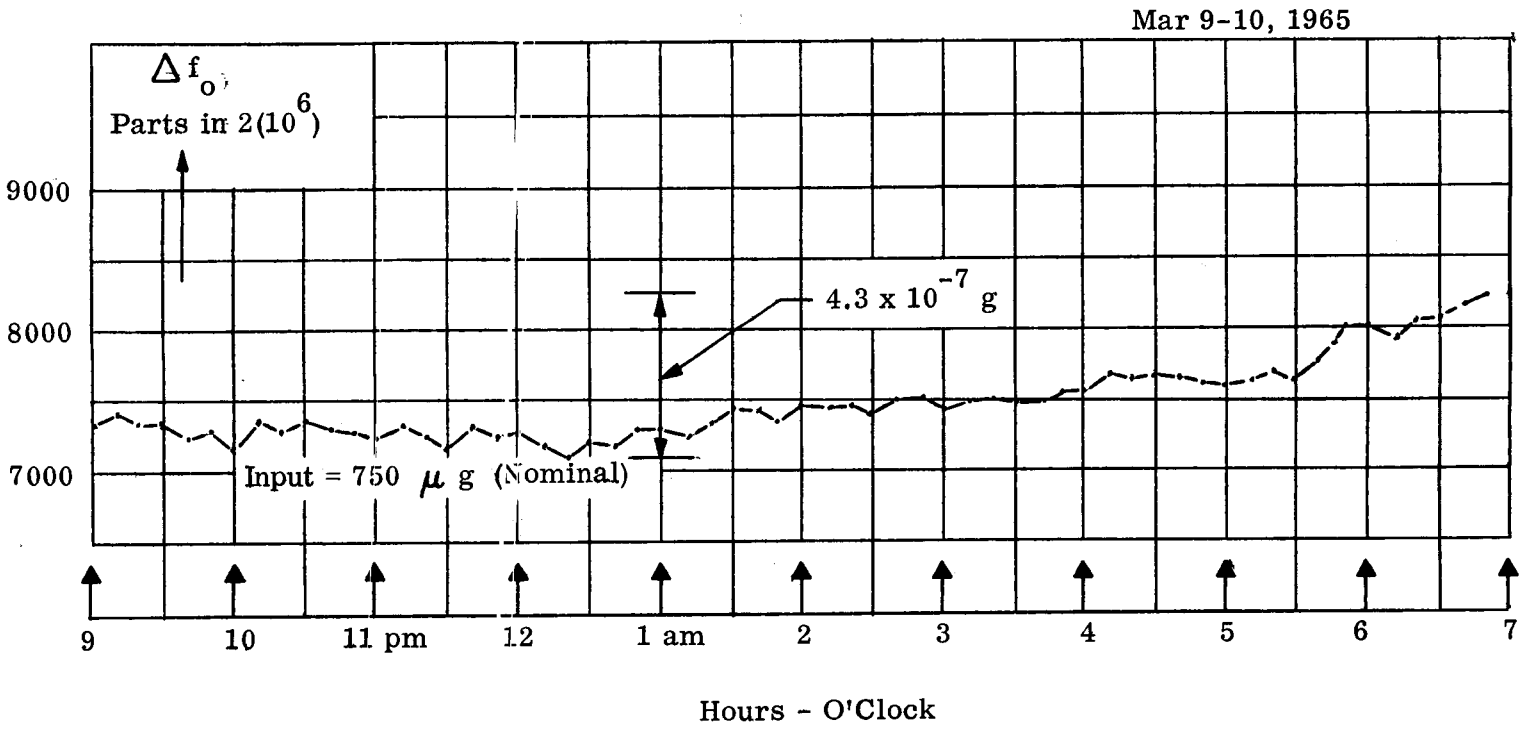

Figure 18. Scale Factor Stability; SN 101 After Environmental Tests

(a) Sinusoidal frequencies shall be swept at a logarithmic rate of two (2) octaves per minute for the three (3) principal axes.

Frequency (cps)	Amplitude (vector g)
5-15	0.4 in. D.A.
15-50	4.5
50-500	6
500-2000	18

(b) Sinusoidal frequencies shall be swept at a rate proportional to frequency in a single axis (because of high amplitude combustion instability phenomena in the thrust axis). This axis will not be the input axis of the accelerometer.

Frequency (cps)	Amplitude (vector g)	Time Duration seconds
550-650	45	30

(c) Gaussian random vibration shall be applied about each principal axis with g peaks clipped at 3 times rms acceleration. Equalization shall be employed to maintain PSD values throughout the frequency spectrum. Rolloff characteristics above 2000 cps shall be 40 db/octave or better.

Frequency (cps)	Duration (min)	PSD (g^2/cps)
20-2000	4	0.07

(d) Shock - three tests to a half sine pulse of 15 g peak amplitude and 10-15 millisecond duration along each principal axis.

Figure 19. Shock Vibration Requirements for Miniaturized Accelerometers when Launched by Thor-Delta Vehicle

SECTION 6.0

CONCLUSIONS AND RECOMMENDATIONS

A concerted analytical, design, fabrication and test effort has been conducted by the Products and Instruments Group of Bell Aerosystems Company to develop a Miniaturized Electrostatic Accelerometer (MESA) for space applications. This accelerometer is characterized by:

(1) Precision digital electrostatic force constrainment along the instrument sensitive axis.

(2) Variable range electrostatic suspension.

(3) The ability to withstand high launch accelerations while nonoperating.

As discussed in the foregoing sections of this report, the instrument has demonstrated significant performance in the critical areas of null and scale factor variations with time and temperature. The program has also pointed out areas where additional study and design improvement should be considered. These are discussed in detail below.

6.1 LOW g TESTING

The evaluation of the MESA performance is limited by current state-of-the-art test instrumentation. The MESA was evaluated on a special test base which exhibited long term stability of 10^{-6} g or better. In order to achieve a test accuracy better than 1% over a range of 10^{-4} to 10^{-6} g, instrumentation errors such as dividing head resolution, repeatability and test base stability must be less than 10^{-6} to 10^{-8} g. Bell Aerosystems has investigated several methods which appear feasible. The practical implementation of these methods would require an additional study and test effort.

6.2 MECHANICAL DESIGN

As discussed in Section 5.1.1, the null bias of the MESA is in the order of 10^{-4} g/g. The machining and measurement of the MESA proof mass tolerances of 10 micro-inches or better is required in order to achieve low null bias. The

present method of measuring float roundness and straightness by mechanical gauges is not accurate enough. The gauge causes deformation of the beryllium cylinder and limits the measurement accuracy. A noncontact method using a capacitive pick-off similar to that used in the MESA has been investigated. It would enable measurements to be made to an accuracy of 1 micro-inch. An improvement by a factor of 10 in null bias to 10^{-5} g/g or lower is possible.

6.3 ELECTRONIC DESIGN

With the availability of many circuit functions in the integrated circuit form, a significant reduction in MESA power, volume, and weight is possible. A preliminary study indicates that the electronics power could be reduced from 8 to 3 watts, volume from 105 to 50 $in.^3$, and weight from 3.8 to 2.0 pounds. The improvements are particularly significant where long term operation of the MESA in a spacecraft is required and where power consumption is important. The reliability also would be improved since fewer components and assembly functions would be required.

Consideration should also be given to simplified and improved system design; in particular:

(1) Elimination of one pulse generator by using electronic switching of pulses and additional logic; results in smaller oven, one less core temperature control and power reduction of two watts.

(2) Use of preregulator in power supply to achieve power conversion efficiency of 90% for input variations of 24 to 34 vdc.

(3) Use of duty cycle modulated temperature controllers; operating efficiency of 90% possible.

(4) Design of automatic suspension recycling control to eliminate possibility of suspension, nonstarting, or dropout during high transient acceleration.

SECTION 7.0

DESIGN REVIEW

The final design review of the MESA dealt primarily with the evaluation test phase, the interpretation of the results as related to the design specifications, and the engineering analyses that established these specifications.

7.1 SYSTEM TEST DATA

The test results demonstrated were well within the specification in all areas except:

(1) Cross-Coupling - The specification (10^{-5} g/g) for cross-coupling effects was not demonstrated primarily because of the state-of-the-art capability for measuring roundness of float. The MESA demonstrated cross-coupling effects approximately an order of magnitude larger than specified.

(2) Power Requirements - The average operating power requirements of 15 watts (specified) is exceeded by approximately 10%.

Recommendations

(1) As mentioned elsewhere in this report, preliminary investigation of using a capacitive pickoff device for mechanical inspection of precise parts appears to be a means of advancing the state-of-the-art and effectively reducing the cross-coupling errors.

(2) The power consumption of the MESA can be reduced to well within requirements by a modification to the temperature control such that it operates in a digital rather than analog mode.

7.2 FAILURES

All failures that occurred during tests were analyzed for cause and the necessary action was taken to correct the problem. A total of six failures occurred, five of which were the same part (Q_2 of the suspension oscillator). Each of the Q_2 (2N834) failures was caused by accidental shorting of the output to ground. To eliminate the problem a resistor and capacitor were added to protect the transistor from accidental shorts. The remaining failure was a power supply transistor

burned out during module testing, and was again induced by the tester and a misplaced test probe.

7.3 SYSTEM OPERATION

During integration and system test, interface and interaction problems resulted in the following design modifications:

(1) In each CTC, a capacitor (1A3C1 and 1A3C2) was added across the bridge to minimize the effect of restoring pulses.

(2) In the suspension amplifier, potentiometer (1A4R11) was added to balance suspension excitation voltage, and fixed capacitor (1A4C6) was added for phase adjustment.

(3) In the output of the ± trigger, resistors (1A4R14 and 15) plus diode (1A4CR12) were added to balance input impedances to multivibrators.

(4) In the two multivibrators, resistors (1A4R5, 6, 7, and 8) were added and the base of the flip-flops was returned to the -16 volt source instead of ground to protect against retriggering on noise pulses.

7.4 SUMMARY

In summary, the final review indicates that the test and evaluation phase generally confirmed the results of the early engineering studies and design decisions. Action taken as a result of the recommendations generated in the design review program served to minimize the system integration and test problems. The detailed engineering associated with the circuit and packaging review, i.e., parts selection and application, thermal and mechanical analyses, in conjunction with the tight quality control program served to respectively eliminate failures during the test program.